# MODELING SURFACE PLASMON RESONANCES OF ARRAYS OF NANO-PARTICLES ON A DIELECTRIC SUBSTRATE USING DISCRETE DIPOLE APPROXIMATION WITH SURFACE INTERACTION (DDA-SI)

A Thesis

by

Zahra Rostampour Fathi

Submitted to the
Graduate School of Sciences and Engineering
In Partial Fulfillment of the Requirements for
the Degree of

Master of Science

in the
Department of Mechanical Engineering

Özyeğin University
June 2017

# MODELING SURFACE PLASMON RESONANCES OF ARRAYS OF NANO-PARTICLES ON A DIELECTRIC SUBSTRATE USING DISCRETE DIPOLE APPROXIMATION WITH SURFACE INTERACTION (DDA-SI)

Approved by:

---

Professor M. Pınar Mengüc, Advisor
Department of Mechanical Engineering
*Özyeğin University*

---

Assis. Prof. Altuğ Başol
Department of Mechanical Engineering
*Özyeğin University*

---

Assoc. Prof. Hakan Ertürk
Department of Mechanical Engineering
*Boğaziçi University*

Date Approved: 19 July 2017

*To: Reza, Ali, Mom and dad*

# ABSTRACT

Analysis of surface plasmon resonance of arbitrary shape nano-particles on a substrate is important for many engineering applications. The strong optical absorption of noble metal nano-particles is due to the localized surface plasmon, which enables the development of novel applications such as surface enhanced Raman spectroscopy based biological sensing, optical transparency based sensors, and uni-directional nano-antennas. Size, shape, and distance between nano-particles on a surface are the key factors in the design of these structure. Usually, these systems utilize noble material such as gold which is deposited on a dielectric surface. Tuning the structures of the noble metals increases the local absorption efficiency of light within specific frequency ranges, depending rely on the final design of the system. Understanding the physics of plasmon phenomena and its relation with these parameters should be studied in depth. This thesis provides a theoretical study and a numerical validation of the coupled phenomena that occurs between gold nano-particles on a dielectric substrate where the nano-particles have different shapes and separation distances. Numerical study of nano-particles on a substrate is carried out using Discrete Dipole Approximation with Surface Interaction (DDA-SI) approach. The DDA-SI is based on the discretization of the nano-particles to dipoles for solving volume integral of Maxwell's equations and Green's dyadic tensor of electric field within the dipoles to calculate the optical properties of arbitrarily shaped, non-homogeneous, anisotropic objects. There are some renowned open sources packages for DDAs. These packages are mostly used for calculating the interaction of particles in a free space with direct wave propagating. However, in order to calculate the light scattering from objects placed on a substrate, the substrate itself also is required to be approximated by the

dipoles which increase the computational time remarkably. In this study, we used the Discrete Dipole Approximation with Surface Interaction (DDA-SI) which is an open source MATLAB based software package for calculation of optical properties of nano-particles (extinction, absorption and scattering) on a substrate. It can be used to investigate both the near- and far-field effects and accounts for the coupling between different particles on the surface.

This study focuses on specific geometries such as cube, spheroid and triangular geometries, each of varying sizes and separation distances from each other. Apart from studying the plasmon resonance of individual nano-particle on a dielectric substrate, a system with more nano-particles is scrutinized. It is found out that as the distance between particles decreases, the plasmon resonance frequency is pushed into the infrared region due to the inter-particle coupling, and the redshift becomes dominant. Furthermore, we found out that the coupling effect becomes negligible if the ratio of their distance between nano-particles to the radius, $c = d/a$, is greater than three.

During this study, the main DDA-SI toolbox is further developed, vecrorized and optimized numerically which named DDA-SI-3 in order to calculate the optical properties of noble metals. The imaginary component of refractive index for noble metals for larger wavelengths is large and make the calculation challenging. Therefore, we applied the new numerical method to calculate the linear system of DDA-SI in order to achieve more precise, faster and stable calculations. The structure of interaction matrix is studied and for this, specific preconditioning matrices are extracted. It is also found out that the use of the least square method, with the proper preconditioning matrices for iteratively solving the linear system, yields results to achieve more accurate and relatively faster calculation.

*Keywords: Surface plasmon resonance, Gold nano-particles, Discrete Dipole Approximation with Surface Interaction (DDA-SI), Surface-particle interaction. iterative methods.*

# ÖZETÇE

Alt malzeme üzeri isteğe bağlı yerleştirilmiş nano parçacıkların yüzey plazmonik rezonans analizleri çoğu mühendislik uygulamaları için önem arz etmektedir. Soy metal nano parçacıkların gösterdikleri güçlü soğurma olayı yüzeyde güçlendirilmiş, Raman spektroskopisi esaslı, biyolojik sensörler, optik saydamlık, esaslı sensörler ve tek yönlü nano antenler gibi birçok özgün uygulamaların geliştirilmesini sağlayan bölgesel hale getirilmiş yüzey plazmonu sonucunda gerçekleşir. Yüzey üzerine yerleştirilmiş nano parçacıkların tasarımındaki kilit unsurlar boyut, şekil ve parçacıklar arasındaki uzaklık parametreleridir. Bu sistemlerde genel olarak dielektrik yüzeye bırakılmış altın gibi soy metallerden yararlanılır. Soy metal yapılarının ayarlanması belirli frekans aralıklarında ışığın bölgesel soğurulma verimliliğini arttırır. Bu çalışmada, her biri farklı boyut ve ayrıklık uzaklığındaki kübik, küremsi ve üçgen biçimli gibi belirli geometriler üzerine odaklanılmıştır. Dielektrik yüzey üzerindeki tekli nano parçacığın plazmonik rezonans çalışmasının yanı sıra birden fazla nano parçacıklı sistemler de irdelenmiştir. Nano parçacıkların ayrıklık uzaklıkları azaldıkça parçacıklar arasındaki kuplaj ve kırmızıya kaymanın domine ettiği ve böylece plazmon rezonans frekans doruğunun kızıl ötesi bölgeye itildiği bulunmuştur. Buna ek olarak, eğer nano parçacıklar arasındaki uzaklığın yarıçaplarına oranı, $c = d/a$, 3ten büyük olursa kuplaj etkisinin ihmal edilebilir olduğunu keşfettik. Bu çalışma boyunca, soy metallerin optik özelliklerinin hesaplanması için asıl kullanılan DDA-SI paketi daha fazla geliştirilerek vektör haline getirilmiş ve numerik olarak optimize edilerek DDA-SI-3 adını almıştır. Soy metallerin kırılma indisinin sanal kısmının uzun dalga boylarında büyük olmasıhesaplamaları zorlaştırır. Bu sebeple, DDA-SI'daki lineer sistemlerin hesaplamalarında daha hassas, hızlı ve stabil sonuçlara ulaşan yeni bir numerik metot

uyguladık. Bu metot ile etkileşim matrisi üzerine çalışıldı ve özel ön düzenleme matrisleri ortaya çıkarıldı. Ayrıca, lineer sistemin tekrarlı(iterasyon) çözümünde en küçük kareler metodunun uygun ön düzenleme matrisleri ile kullanılması sonucunda daha kesin ve görece daha hızlı hesaplamaya ulaştığı keşfedildi.

*Kılavuz/anahtar sözcükler: Yuzey Plazmon Rezonansı, Altın nano parçacıklar, Yuzey Etkileşimi ile Ayrık Dipol Yaklaşıklama, uzey-parçacık etkileşimi, iterasyon yöntemleri.*

# ACKNOWLEDGEMENTS

Foremost, I would like to express my sincere gratitude to my advisor Professor M. Pınar Mengüc, for intruducing me this interesting topic as my thesis. Furthermore, I profound gratitude to Mert Kaya whose without helping him, studying my Master at Ozyegin University was impossible.

I would like to thank my wonderful family for believing in me and supporting my decisions and to my brother who has been always will be the color of my life.

Finally, I must express my very profound gratitude to my spouse Reza Pakdaman Zangabad for providing me with unfailing support and continuous encouragement throughout my years of study in Istanbul far away from him and through the process of researching and writing this thesis. This accomplishment would not have been possible without him. Thank you.

# TABLE OF CONTENTS

# LIST OF TABLES

# LIST OF FIGURES

# CHAPTER I

# INTRODUCTION

The advent of nanotechnology has allowed scientists to study light-matter interactions at the nanoscale sizes. A significant amount of fundamental knowledge has accumulated in the past decade and the field of nano-optics may now in fact be on the cusp of delivering on practical applications in a variety of fields. Nanotechnology can be understood as the design, characterization, production and application of structures, devices and systems by manipulating size and shape at the nanoscales [5]. The main driving force behind all these studies is the desire to fabricate materials that are likely to impact practically all areas related to different applications, biomedical sciences and other multidisciplinary fields of science and engineering. Nanoscale size particles can be considered as a number of atoms or molecules bonded together (these particles usually include $10^6$ atoms or fewer) and are intermediate in size between single atoms and aggregates large enough to be called bulk material [6]. Therefore, nanoscale size materials show behaviors that are intermediate between that of a macroscopic solid and the atomic or molecular systems. For instance, metal nano-particles (NPs) have unique optical and electronic properties that are exactly distinguished from those of the individual atoms as well as their bulk doublet. The optical phenomena related to the electromagnetic response of metals, led to the improvement of an emerging and rapid growing research field named plasmonics.

The structure of metals can be assumed as a gas of free electrons in a lattice of positively charged ions. If the electron gas is in equilibrium; the amount of negative and positive charges will be equal in the metal lattice space, so the net charge density is zero. However, when the noble metal structure is disturbed from equilibrium by

incident electromagnetic (EM) wave, there will be a net non-zero charge density. Therefore, in order to keep charge neutrality in the system, an internal electric field is created. Because of the incident EM wave, the conductive electrons start to oscillate with the same frequency of the EM wave. On the other hand, the mass of the metal ions is larger than the mass of the conductive electrons, so the electrons move against a background of stable ion lattice. The conductive electrons cause moment from the EM wave, and thus oscillate around their equilibrium position. This collective, longitudinal oscillation of the conductive electron gas in the metal structure is named a plasma wave [7]. The quantization of these plasma waves is called the plasmon. The reason of the light absorption by metal NPs is the coherent oscillation of the conductive electrons resonance by the incident EM wave as shown in Figure 1.

These structures are characterized by the field enhancement at the interface, while the EM wave vector decays exponentially away from the surface (in the nanometer range), resulting in a very strong local enhancement electric field [8]. Plasmon resonances lead to strong localized near fields at defined wavelengths. The near field enhancement and absorption bands will be shifted to other wavelengths, depending on the kind of shape, geometry and distance of the NPs [9]. Near the resonant frequencies, the absorption between the NPs is enhanced dramatically and can enable designing a tunable structural for photovoltaic applications [10]. The most common plasmonic particles such as gold (Au) and silver (Ag) NPs have remarkable optical, electrical, and thermal properties associated with surface plasmons that make them beneficial in a wide variety of applications [5]. For noble metals, plasmon resonance occurs in the visible - near ultraviolet (UV) if the size of the particle is smaller than the electron mean free path [11]. The mean free path is a measurement of the average distance between sequential collisions of energy carriers. In the case of metals, the electron mean free path $l_{mfp}$ is an important factor because electrons are the energy carriers [12].

Nano-particles have been characterized by a various optical methods, containing absorption spectroscopy and by structural probes like Atomic Force Microscopy (AFM) and Scanning tunneling microscope (STM) [13]. The purpose of AFM technique is to recognize NP between tip to find an optimized location to move the probe in order to selectively heat AuNPs [4]. Because only the absorption NP are presented, they can be converted to localized heating rates either using macro-scale radiation transfer calculations [14] or by adapting near-field calculations similar to those reported by Francoeur and Menguc [15].

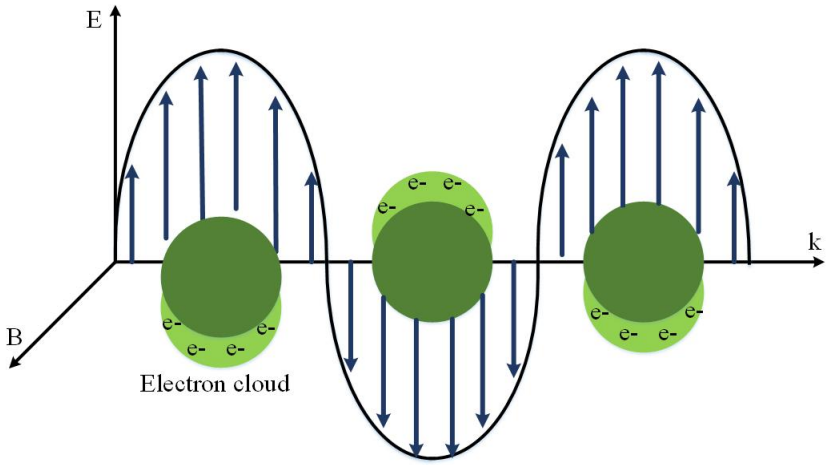


**Figure 1:** Localized surface plasmon resonance (LSPR), resulting from the collective oscillations of delocalized electrons in response to an external EM wave.

The localized surface plasmon has been utilized in a wide range of applications, including magneto-optical rotation (Kerr rotation and Faraday rotation) [16], enhanced fluorescence [17] and surface enhanced Raman scattering [18]. The development of new fabrication technology toward achievement of the optical properties of the gold nano- dimers and nano-trimers with different shapes on a substrate have already been studied experimentally and compared with theoretical predictions [19] and bench marked by numerical methods like DDA [20], finite difference time domain (FDTD) [21] and Finite Element Method (FEM) [22].

## *1.1 Absorption and Scattering of Light*

When an EM wave incidents on an object, the conductive electrons can convert the energy from the incident EM wave into thermal energy. This phenomena is called the absorption process. In this case the energy is transferred to the form of thermal energy or stored in local, non-radiative fields near the object (the near field). However, the conductive electrons can also be accelerated so they can radiate energy in all directions, so called scattering process. Scattering is a process that does not remove energy from the radiation field, but may redirect it. Extinction is a process that decreases the radiant intensity and is due to absorption and scattering.

When an object is placed within a beam of EM wave, a detector that is deviated from the direction of propagation of the incident wave will only receive the radiation scattered by the object. A detector placed within the beam "downstream" from the object will detect that part of the beam which remains unaffected by the object. This part of the incident EM wave is called transmitted radiation, and if the transmitted energy is less than the energy incident on the object, it is said that the object has caused extinction of the EM wave. The difference between incident energy and the sum of transmitted and scattered energy is computed for the absorption (Figure 2).

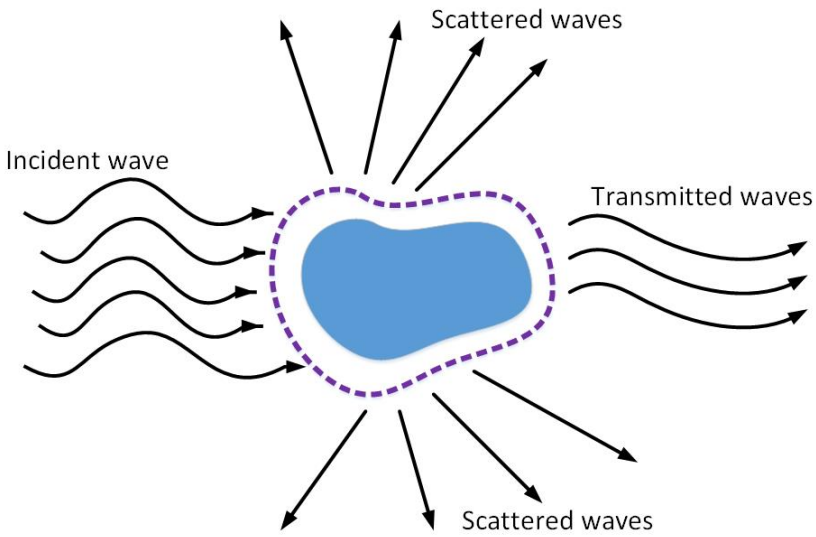


**Figure 2:** Illustration of the absorption, scattering and transmitted of the EM wave by an arbitrary shape particle.

## *1.2 The Calculation Methods of Light Scattering Problem*

Manipulating and governing of light-matter interaction at the nanoscale size is one of the effective techniques enabled by advances in the nanotechnology fabrication and improvement of the numerical methods for solving the light scattering problems. Light scattering by particles is related to many practical applications, including interstellar dust, ice crystals in atmosphere and plasmonics. In general, interaction of EM wave with matters is identified by solving Maxwell's equations. However, analytical solution of Maxwell's equations is limited to some basic geometries like spheres. Because it is generally impossible to solve Maxwell's equations for light scattering problems from arbitrarily shape and anisotropic practical analytically, therefore semi-analytical and numerical methods are needed to be developed. On the other hand, numerical methods must deal with computational problems for complex shaped particles and produce reliable results. There are a number of available numerical methods that have been developed to compute the scattering of EM wave radiation by different

shape particles. Below some important methods are given and their advantages and disadvantages are discussed:

1) Discrete Dipole Approximation (DDA)

2) Finite Difference Time Domain (FDTD)

3) Finite Element Method (FEM)

4) T-Matrix Method (TMM)

5) Ray-Tracing Method (RTM)

**Discrete Dipole Approximation (DDA):** is the most effective method to compute scattering and absorption of EM waves by arbitrary shape and composition particles with sizes smaller than or comparable to the wavelength of incident EM wave. Its concept consists of dividing a particle into polarizable point arrays located on a cubic lattice. In response to the incident EM wave, each point behaves as a hertzian dipole so the scattering problem can then be solved as a summation of linear equations of dipole moments. DDA calculations require choices for the locations and the polarizabilities of the dipoles that representing the target. Extension of this method allows calculating light scattering by periodic objects, arbitrarily shaped, inhomogeneous targets placed on a surfaces [23] [2] [24].

**Finite Difference Time Domain (FDTD):** is discretization method of time and space for solving the light scattering problem of particles with complex geometries and compositions by defined derivatives in the Maxwell curl equations replaced by finite difference quotients. In this method, the region including a scattering particle is discretized by using a mesh grid. Furthermore, the existence of the particle is represented by assigning suitable electromagnetic constants in terms of permittivity and conductivity applied by a Drude-Lorentz model [25].[26]

**Finite-Element Method (FEM):** is based on solving the scattering problem in the frequency domain by modeling of the discretization of the Helmholtz equation at boundary of the particle surface. This method can be used to calculate the light

scattering from arbitrarily shaped, inhomogeneous and anisotropic particles for a single frequency at a time. The particle is embedded in a finite computational domain that is discretized into many small volume cells with about 10 to 20 elements per wavelength. A suitable grid element for example, triangular and tetrahedral can be used to represent the surface or structure, with the continuity conditions required at adjacent grid cells. This method needs to discretized not only the particle but also the space around it[25] [27].

**The Ray-Tracing Method (RTM):** is an approximated method for calculation of light scattering by the particles much larger than the wavelength of incident EM wave. The basic assumption of ray-tracing method is combination of ray-tracing and Monte Carlo techniques in which the incident EM wave can be represent as a collection of independent parallel rays by using a Monte Carlo model. In the ray tracing method diffraction theory and the Fresnel reflection and transmission equations are applied [25] [28].

**T-Matrix Method (TMM):** is the calculation of optical properties of the particles with rotationally symmetric shape (such as spheroids, circular cylinders, etc.) In this method, the incident and scattered EM waves are developed in vector spherical wave functions. The elements of the T-matrix are dependent only on the size parameter, shape and refractive index of the particle and on its orientation. However they are independent of the incident and scattered fields. The T-Matrix transforms the expansion coefficients of the incident field into the scattered field which can be used to calculate any scattering problems of a non-spherical particle. Several T-Matrix codes for solving the light scattering problem by rotationally symmetric particles in both stable and random orientations are available on the open source softwares [25] [29].

The comparisons of the advantages and the disadvantages of the maintained computational techniques to model the scattering of EM wave from metal nano-structures

are listed in the Table 1. The size parameter is the dimensionless

$$x = \pi D/\lambda \tag{1}$$

where $D$ is the characteristic size of the particle and $\lambda$ is the wavelength of incident EM wave.

**Table 1:** List of numerical methods

| ***Numerical Methods*** | ***Abbreviations*** | ***Advantages*** | ***Disadvantages*** |
|---|---|---|---|
| Discrete Dipole Approximation | DDA | Any shape and composition, possible to include a substrate interaction | Convergence criterion: $nkd$ <1 (There is restriction to solve large refractive index) |
| Finite-Difference Time-Domain Method | FDTD | Any shape and composition include a substrate interaction | Limited range of size parameters (up to x =15-20), less accuracy |
| Finite-Element Method | FEM | Any shape & more accurate | computationally slow |
| Ray-Tracing Method | RTM | Applied to any shape (spherical or non-spherical) | Approximated method (limited range of size parameters) |
| T-Matrix Method | TMM | Highly accurate ; computationally fast; Possible to include a surface interaction; (multilayered) spheres. | Limited types of particle shapes; Limited range of size parameters (x<30); (the matrices are truncated) |

## *1.3 Selected Method for This Study*

In this thesis,the DDA is selected as the methodology to calculate the light scattering and absorption problem. In principle, the DDA allows for the consequent computational over-heads, which is capable of treating targets of arbitrary geometry and optical properties. Due to the flexibility associated with the description of the system to be simulated, the DDA has been employed to calculate the optical properties associated with non-spherical and inhomogeneous particles.

This thesis is broken down into the following chapters; Chapter II contains the review of the DDA, briefly discussing the theory and structure of the DDA. In the Chapter III, we introduce the DDA in the presence of a surface (DDA-SI). Also this Chapter contains the iterative methods for solving the DDA-SI linear equation. In the Chapter IV we validated the accuracy of the selected method (DDA-SI) by computing absorption efficiency of a single 50 nm cube on the BK7 substrate with the results of the FEM. In the following Chapter, we provide detailed investigation of the plasmon resonance of kinds of nano-structures such as AuNPs have been investigated, including nano-spheres, nano-cubes as well as dimers and trimers containing sphere-cube geometries, to understand their localized surface plasmon resonance (LSPR) spectrally. Chapter IV discusses in brief what the results entail followed by the conclusions and proposed future research direction.

# CHAPTER II

# DISCRETE DIPOLE APPROXIMATION WITH SURFACE INTERACTION (DDA-SI)

In this thesis, the DDA-SI is a chosen method as a calculation tool. The main advantage of this method is its development for calculation of scattering of different shape particles on a surface. Light scattering problem based on DDA-SI method is validated and bench marked with the other methods [30]. DDA-SI is further optimized, vectorized and particularly the computational efficiency is improved.

## *2.1 Introduction*

The Discrete Dipole Approximation (DDA) is an accurate numerical method to calculate electric enhanced effect, EM scattering and optical properties of an individual or multiple scatterers of different shapes. It is also referred as the coupled dipole method (CDM) [31]. For the first time, DeVoe [32] used the DDA method in studying the optical properties of the accumulation of molecules. However, the retardation effects were not included in the calculation making his method limited to aggregates that were small compared with the wavelength. Purcell and Pennypacker [33] implemented the retardation effects in the DDA method in order to study the interstellar dust grains and aerosols. Later, Draine and Flatau popularized the method by developing an open source computer code called DDSCAT which was written in FORTRAN [23] [34]. These methods are widely used for simulating the EM wave and particles interaction in free space with direct propagating waves and had the capability of approximating the scattering object by an array of point dipoles (Hertizan dipoles)[33]. These dipoles interact with each other and the incident electric field giving rise to a

linear system of equations that obtain the polarizations at each dipole. Dipole interactions are approximated based on the volume integral equation for the electric field. McDonald et al.[35] named *Open DDA*. In addition, Yurkin et al. [24] [36] developed open-source DDA packages written in the *C* language and named *Amsterdam DDA (ADDA)*. for modeling the interaction of EM wave with objects in free space. In order to model the light scattering from particles on a planar surface, Taube blatt and Tran [37] added the surface interaction capability in their Fortran implementation of DDA and lately Schmehl et al.[38] implemented DDSURF also written in FORTRAN by modeling the light scattering from particles on a semi-infinite surface. Recently Yurkin added surface interaction to their ADDA toolbox [39]. Loke and Menguc [2]. developed DDA-SI which is an open-source and MATLAB software package based on the analyses of Schmehl [38] containing DDA with surface interaction and applied for light propagating from particles on the substrate. The DDA-SI also has the capability of analyzing and simulating the far-field scattering by objects on a surface which are illuminated by an evanescent wave and created by total internal reflection which is quantified by the Mueller matrix elements. Manickavasagam et al [40] calculated the scattering Muller matrix from soot agglomerates. Furthermore, Short at el. [41] calculated the muller matrix and implemented it into the DDA-SI toolbox. The accuracy and results of the DDA-SI toolbox was compared with FEM and FDTD methods [30]. Recently, Moghaddam et al [3] vectorized the main toolbox of DDA-SI for making it faster. The history of DDA development is presented in Table 2.

The DDA starts by dividing the scattering object into $N$ polarizable point dipoles which is denoted in Figure 3. There is no restriction on the localization of the dipoles, which means that the DDA can represent a particle of arbitrary shape and composition. However, there are three basic criteria in the discretization of particle to dipoles:

I. Required number of dipoles for accurately approximation of the NP.

**Table 2:** A Historical development of DDA

| ***Name*** | ***Reference & Authors*** | ***Language*** | ***Year*** | ***Short Description*** |
|---|---|---|---|---|
| *DDSCAT* | B.T. Draine & P.J. Flatau [23] | FORTRAN | 1988<br>2012<br>2015 | Calculates scattering and absorption of EM waves by particles of arbitrary geometry and periodic particles -Compute the near field and far field. No surface interaction. With 2D FFT. |
| *Open-DDA* | McDonald[42] | C | 2007 | Absorption of EM waves by arbitrary shape particles. With FFT. No surface interaction |
| *DDASURF* | R. Schmehl, B. M. Nebeker [43] | FORTRAN | 1997 | Calculates scattering and absorption of EM waves by particles of arbitrary shapes on or in proximity to a surface. 2D-FFT is used. Not released. |
| *ADDA* | M.Yurkin, A. G. Hoekstra [36] | C | 2007 | Calculates scattering and absorption of EM waves by particles of arbitrary geometry on the surface with FFT. |
| *DDA-SI* | V. L. Y. Loke M.P. Menguc [2] | MATLAB | 2012<br>2013<br>2014 | Calculates scattering and absorption of EM waves by particles of arbitrary geometry on or in proximity to a surface. No FFT acceleration is used. |

II. Accuracy of the method for different size, complex refractive index $m$, and wavelength $\lambda$ of incident EM wave.

III. Proper numerical method for solving linear equation of the unknown moment $P$.

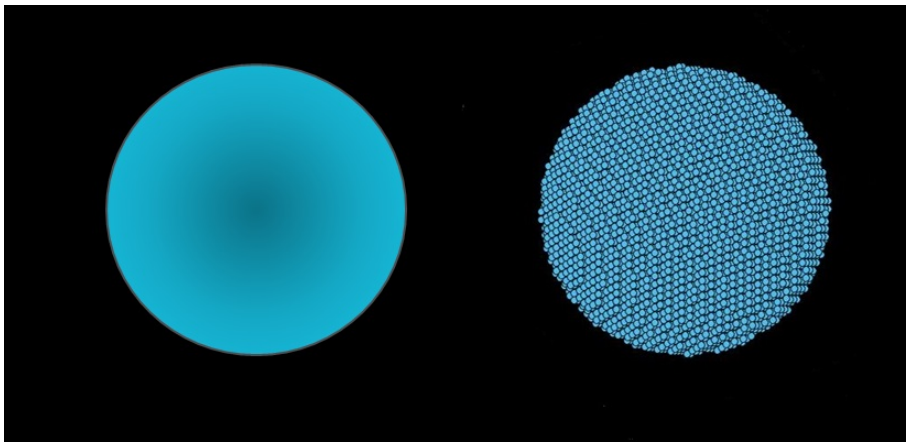

**Figure 3:** Discretization of sphere to point dipoles with number of dipoles( $N = 14328$).

## *2.2 Dipole Coordinates*

At the first step we assume the scattering object is divided in to point dipoles where their size are smaller than the incident wavelength (Rayleigh scatterers), numbered $j = 1, ..., N$ with polarizabilities $\alpha_j$ (Due to incident EM wave and interaction with other dipoles) located at positions $r_j$. The variable $r$ is an $N \times 3$ array matrix, the standard DDA uses the Cartesian coordinate system and the dipoles are packed in a cubic lattice.

Figure 4 shows the discretization of cube and sphere to point dipoles $N_{cube} = 13824$ and $N_{sphere} = 14328$ with the same volumes to represent the scatterer. The dipoles must be packed in the minimal lattice spacing which is determined by Draine and Flatau [23]. The relationship of the volume of discretized sphere and lattice spacing is:

$$Volume = \frac{4}{3}\pi r^3 \equiv N(Latticespacing)^3 = Nd^3 \tag{2}$$

The fundamental premise of this method is that the volume of the object is broken down into a representative array of $N$ dipoles arranged in a cubic lattice, with spacing

$d$ and the volume of the equivalent sphere with effective radius $a$ :

$$a = d(\frac{3N}{4\pi})^{1/3} \tag{3}$$

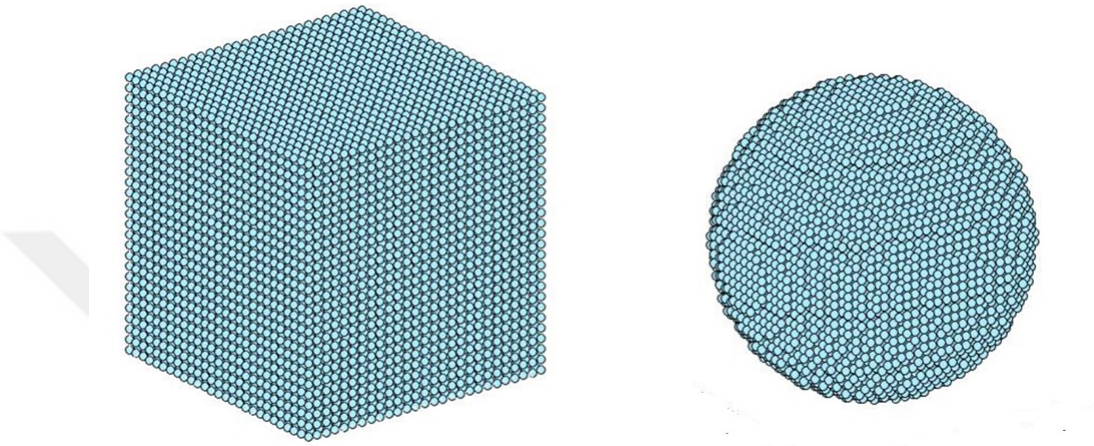

**Figure 4:** Sample of cube and sphere with the same volume discretized to dipoles $N_{cube} = 13824$, $N_{sphere} = 14328$.

Based on these parameters, the associated suggestion for two essential criteria can be employed in the DDA calculation in order to achieve a sufficient and reasonable accuracy as it shown in Figure 5. In general, there are two important requirements on the application of DDA to solve light scattering problem by Rayleigh particles:

1. The equation $d \leq 1/|m|k$ (where $m$ is the complex refractive index, $k$ is a wave vector of the incident wave, and $d$ is the dipole spacing) must be satisfied so that $d$ must be small enough compared to the wavelength of the incident light.

2. Either $d$ must be small enough or $N$ large enough such that the objects are accurately depicted with the lattice of dipoles.

Another important restriction of the DDA calculation is for the case of an object composed of noble material. When applying the DDA to such a noble particle, we have to be sure that the dipoles forming the scatterer particle remain electric dipoles,

means that the relative contribution of the dipole moment to the light scattering is adequately small. Last significant factor of the DDA calculation has had effect on the speed of calculations as well as on the accuracy of the results.

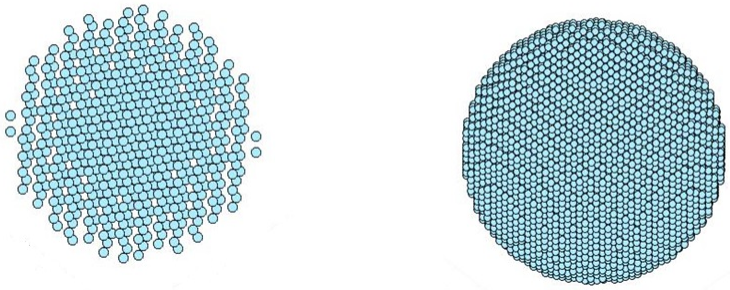

**Figure 5:** A single sphere with $N = 552$ dipoles number (Right); A single sphere with $N = 17256$ dipoles number (right) when size parameter is $x = 0.25$.

## *2.3 Complex Refractive Index*

Second step in the DDA-SI calculation is expressed as a function of the refractive index $m$ with respect to the surrounding medium. It means that the accuracy of DDA calculation also does depend on the complex, frequency dependent refractive index $m$ which describes how strongly the electric dipoles react to the incident field [44] and could be defined as:

$$m = n + i\kappa \tag{4}$$

The real part $n$ indicates the refraction of incident light (equals the speed of light in vacuum divided by the speed of light in the metal $n = c_0/c$), and the complex part of the refractive index, $\kappa$ is called the extinction coefficient and determines the optical absorption of EM wave propagating through the medium($cm^{-1}$) by using the following equation [45]:

$$Absorption\ efficiency = \frac{4\pi\kappa}{\lambda} \tag{5}$$

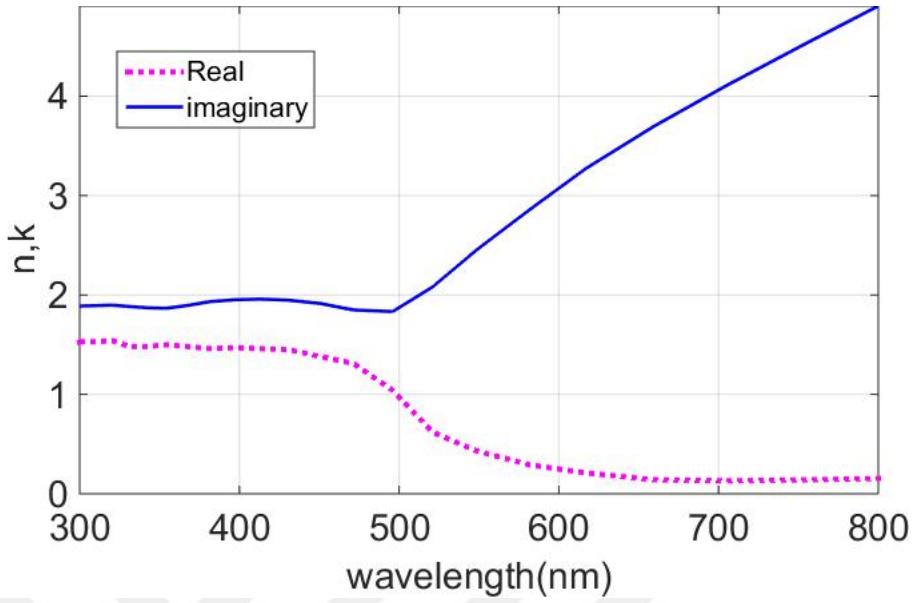


**Figure 6:** The real and imaginary part of the refractive index of Au at visible light range [1].

The value of $\kappa$ is not exactly zero for any material, but materials with a value approaching to zero are dielectric materials. As needed for the calculation of the Rayleigh criteria in the DDA approximation, the magnitude of the refractive index, $m$ is calculated by:

$$|m| = \sqrt{n^2 - \kappa^2 + 2in\kappa} \tag{6}$$

The experimentally obtained optical constants of noble metals are given by Johnson and Christy [1]. Figure 6 shows the dispersion of the refractive indices of Au used in the models is calculated using the Drude-critical [46]. As it is obvious from Figure 6, the imaginary part of refractive index for Au is increased by increasing the wavelength. Figure 7 shows the refractive index of BK7 glass using the Sellmeier equation. [47]. The Sellmeier equation is used to characterize the dispersion of light with respect to wavelength and is written in the form:

$$n^2(\lambda) - 1 = \frac{B_1\lambda^2}{\lambda^2 - C_1} + \frac{B_2\lambda^2}{\lambda^2 - C_2} + \frac{B_3\lambda^2}{\lambda^2 - C_3} \tag{7}$$

where $\lambda$ is wavelength in m and $B_1$ , $B_2$ , $B_3$ , $C_1$ , $C_2$ , and $C_3$ are constants unique to the material being tested.

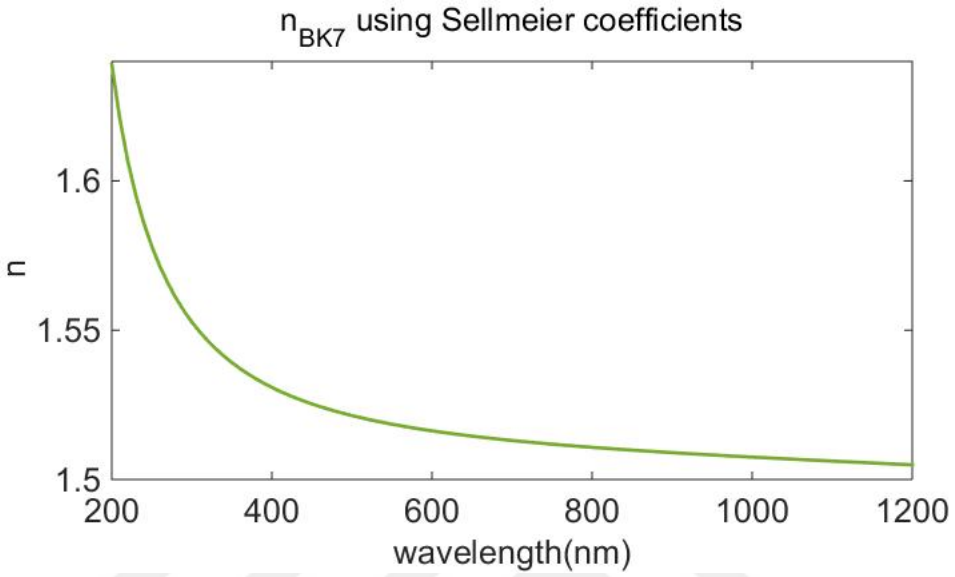


**Figure 7:** Refractive index of the BK7 glass calculated using the Sellmeier equation.

## *2.4 Electric and Magnetic Field Expressions*

We assume the scattering particle is non-magnetic.The DDA is thoroughly applicable to any incident field; however, for simplicity we assume a monochromatic plane wave with unit amplitude. Each of dipoles is excited by a monochromatic incident plane wave $E_{inc}$:

$$E_{inc}(r,t) = E_0 \exp(ik.r - i\omega t) \tag{8}$$

Where $r$ is the position vector, $k$ is wave vector ($k = \omega/c = 2\pi/\lambda$) and $E_0$ is the amplitude of the incident wave. For simplicity the $\omega$ dependence on all quantities is omitted. Thus the moment of each dipole as a result of the interaction with the incident electric field $E_{inc}$ and re-radiating from other dipoles will be: $P_j = \alpha_j E_j$, where $E_j$ is the electric field at $r_j$ due to the incident wave, plus the contribution of

each of the other $N-1$ dipoles:

$$E_j = E_{inc,j} + E_{dip,k} = E_0 e^{ik.r_j} - \sum_{j \neq k} A_{jk}.P_k \tag{9}$$

where $A_{jk}$ is the tensor that represents the interaction between the receiving dipole at $r_j$ and the radiating dipole at $r_k$. The electric field from a radiating electric dipole is defined:

$$E = \frac{1}{4\pi\varepsilon_0}\left\{k^2(\hat{r}\times p)\times\hat{r}\,\frac{e^{ikr}}{r} + [3\hat{r}(\hat{r}\times p) - p]\left(\frac{1}{r^3} - \frac{ik}{r^2}\right)e^{ikr}\right\} \tag{10}$$

which is derived from Maxwells equations.Using the vector identity $(r \times p) \times r = p(r.r) - r(r.p)$, we obtain the block off-diagonal $3 \times 3$ interaction tensor defined in Draine and Flatau [48],

$$A_{jk} = \frac{\exp(ikr_{jk})}{r_{jk}} \times \left[k^2(\hat{r}_{jk}\hat{r}_{jk} - I_3) + \frac{ik\hat{r}_{jk} - 1}{r_{jk}^2}(3\hat{r}_{jk}\hat{r}_{jk} - I_3)\right]; \quad j \neq k \tag{11}$$

where $I_3$ is the $3 \times 3$ identity matrix, $r_{jk}$ is the distance from point $r_j$ to $r_k$ and $\hat{r}_{jk}$ is the unit vector direction from points $r_j$ to $r_k$. The dipole interaction tensor $A_{jk} = k^2 G_{jk}$ is related to the Green's tensor $G_{jk}$ of the electric field from the radiating dipole, defining self-interacting $A_{jj} \equiv {\alpha_j}^{-1}$ reduces the scattering problem to finding the polarizations that satisfy a system of complex linear equations, by simplified two matrices[48]:

$$\sum_{k=1}^{N} A_{jk} P_j = E_{inc,j} \tag{12}$$

## *2.5 Polarizability*

The fundamental implementation of the DDA is the Clausius-Mossotti relation (CMR) to define the dipole polarizabilities. In this method, the polarizability $\alpha$ is describing by the bulk optical properties of the scattering particle meaning that it is a function of the complex refractive index $m$ define as:

$$\alpha_{CMR} = \frac{3d^3}{4\pi}\left(\frac{{m^2}_j - 1}{{m^2}_j + 2}\right) = \frac{3d^3}{4\pi}\left(\frac{\in_j - 1}{\in_j + 2}\right) \tag{13}$$

This approach is also correct in the infinite wave length limit of the DDA, $kd \rightarrow 0$. Draine showed that for finite wavelengths, the optical theorem requires that the polarizabilities include a radiative-reaction correction of the form [49]:

$$\alpha = \frac{\alpha^{(nr)}}{1 - (2/3)i(\alpha^{(nr)}/d^3)(kd)^3} \tag{14}$$

where $\alpha^{nr}$ is the non-radiative polarizability which before any radiative-reaction correction is applied. [48]. The current most popular form, the lattice dispersion relation (LDR), was derived by Draine and Goodman[49] which is used in DDA-SI toolbox:

$$\alpha_j{}^{LDR} = \frac{\alpha_j{}^{CM}}{1 + \frac{\alpha_j{}^{CM}}{d^3}\left[(b_1 + m^2 b_2 + m^2 b_3 S)(kd)^2 - \frac{2}{3}i(kd)^3\right]} \tag{15}$$

$\mathrm{b_1}$ = -1.891531, $\mathrm{b_2}$ = 0.1648469, $\mathrm{b_3}$ = -1.7700004,

$S$ is a function of the propagation direction and polarization of the incident wave.

$$S \equiv \sum_{j=1}^{3} (\widehat{a}_j \widehat{e}_j)^2 \tag{16}$$

Where $\hat{a}$ and $\hat{e}$ are the unit propagation and polarization vectors, respectively. Note that Eq.15 gives $S = 0$ for waves propagating along any of the lattice axes. For anisotropic particles, the polarizability of each dipole can be different in the $x$, $y$ and $z$ directions and also for inhomogeneous materials various from the each other.

The values of polarizability are arranged in the similar sequence as the dipole coordinates. However, they are transposed from $N \times 3$ to the $3N \times 1$ array of $\alpha_{x1}$ , $\alpha_{y1}$ , $\alpha_{z1}$ , $\alpha_{x2}$ , $\alpha_{y2}$ , $\alpha_{z2}$ , ..., $\alpha_{xN}$ , $\alpha_{yN}$ , $\alpha_{zN}$ , so that the diagonal of interaction matrix can be fitted into inverse polarizabilities by the matrix when setting Eq.9 into Eq.12. The field $E_j$ at a particular dipole causes it to be polarized or acquire a dipole moment $P_j$:

$$P_j = \alpha_j E_j \tag{17}$$

In the DDA-SI calculation, we chose the LDR approach to obtain a polarizability prescription that accounts both for finite wavelength and for local field corrections arising from target geometry [49].

## 2.6 Constructing the Interaction Matrix

The interaction matrix is created by chaining from dipoles $j = 1...N$. The self-interaction of a dipole is just the reciprocal of its polarizability as shown in Figure 8. Furthermore, the block off-diagonals are the Green's tensors for the interacting dipoles at $r_j$ and the radiating dipoles at $r_k$ , $k = 1...N$, In general, the interaction matrix (DDA Matrix) is defined as [23]:

$$A_{jk} = \frac{k^2 \exp(ikr_{jk})}{r_{jk}} \begin{bmatrix} \beta_{jk} + \gamma_{jk}\widehat{r}^2_{jk,x} & \gamma_{jk}\widehat{r}_{jk,x}\widehat{r}_{jk,y} & \gamma_{jk}\widehat{r}_{jk,x}\widehat{r}_{jk,z} \\ \gamma_{jk}\widehat{r}_{jk,y}\widehat{r}_{jk,x} & \beta_{jk} + \gamma_{jk}\widehat{r}^2_{jk,y} & \gamma_{jk}\widehat{r}_{jk,y}\widehat{r}_{jk,z} \\ \gamma_{jk}\widehat{r}_{jk,z}\widehat{r}_{jk,x} & \gamma_{jk}\widehat{r}_{jk,z}\widehat{r}_{jk,y} & \beta_{jk} + \gamma_{jk}\widehat{r}^2_{jk,z} \end{bmatrix}; \qquad j \neq k \qquad (18)$$

$$A_{jk} = \frac{1}{\alpha_j} I$$

Matrix $A_{jk}$ is complex-symmetric if and only if $\alpha_j$ is complex- symmetric for all $j$.

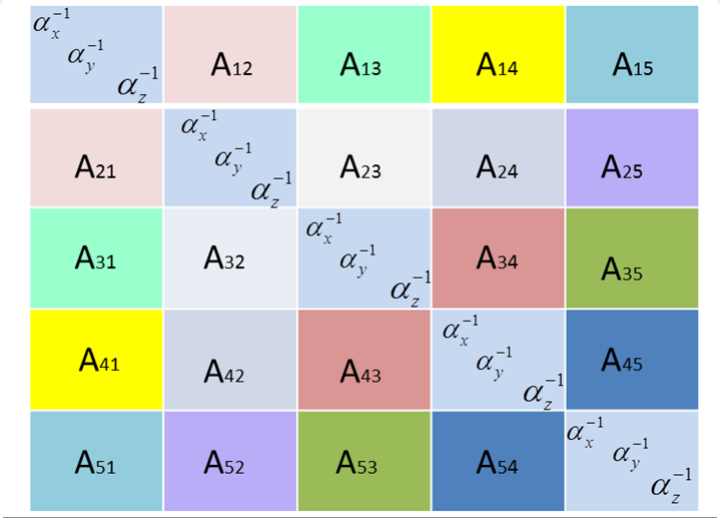


**Figure 8:** Structure of the interaction matrix ($A$) for an isotropic NP in free space.

To solve the linear system of Eq.17, the properties of the coefficient matrix (total interaction matrix) plays an important role, so it is required to be investigated extensively. The interaction matrix for the isotropic particles is symmetric and the

diagonal elements are equal because they are constructed of self-polazibility. Furthermore, dipoles interact with each other in the array, with the strength of the interaction depending on the direction and distance. Therefore, each element of matrix in row is transpose of elements in the column as is depicted in Figure 8.

## *2.7 Extinction, Scattering and Absorption Cross-sections*

Once the dipole moments $P_j$ calculated, the extinction and absorption cross sections can be obtained. The extinction for particle is calculated using optical theorem and absorption cross sections can be calculated by summing over the rate of the energy dissipation by each of the dipoles, as defined by Draine [48]:

$$C_{ext} = \frac{4\pi k}{|E_0|^2} \sum_{j=1}^{N} \mathrm{Im}\left(E^*_{inc,j}.P\right) \tag{19}$$

$$C_{abs} = \frac{4\pi k}{|E_0|^2} \sum_{j=1}^{N} \left\{ \mathrm{Im}\left[P_j.(\alpha_j^{-1}) * P_j^*\right] - \frac{2}{3}k^3|P_j|^2 \right\} \tag{20}$$

The scattering cross section can be obtained from the difference of extinction and absorption cross section $C_{sca} = C_{ext} - C_{abs}$. These quantities are often expressed in terms of extinction, absorption and scattering efficiencies, the cross section divided by the cross sectional area of the scatterer. In the case of a sphere, the extinction efficiency is defined as $Q_{ext} = C_{ext}/(\pi a^2)$, where $a$ is the radius of the sphere. Similarly, the absorption and scattering efficiencies are defined, respectively, as: $Q_{abs} = C_{abs}/(\pi a^2)$ and $Q_{sca} = C_{sca}/(\pi a^2)$.

## *2.8 DDA with Surface Interaction (DDA-SI)*

For the calculation of scattering and absorption of EM waves when the object is on a substrate, we have to observe three situations. Primly, when the illumination of EM wave originates from the same medium where the object resides, the incident field results from the superposition of the direct and reflected incident light (Figure 9). In addition to the direct dipole-dipole interactions in standard free space DDA, we will

have to include the surface-reflected interactions in the presence of surface. Finally, when for the calculation of the scattered field, the reflected component needs to be included. DDA-SI is also capable of simulating the near and far-field scattering by objects on a surface illuminated by an evanescent wave and created by total internal reflection, Loke et el. [2]. Moghaddam et el. calculated the absorption of a sphere and core shell Au nano-sphere on a dielectric surface under an AFM prob [3][50].

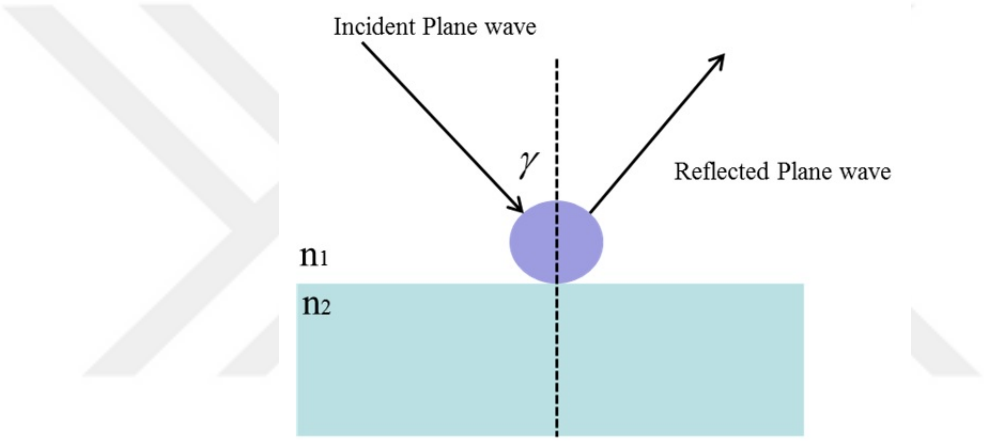


**Figure 9:** A particle illuminated by the direct plane wave incidents at the angle $\gamma$ and the reflected plane wave.

## *2.9 Interaction Matrix in the Presence of a Substrate*

In the presence of a surface, the Green's tensor for a dipole-dipole interaction will have two components; the system of linear equations for DDA-SI is [2]:

$$\sum_{k=1}^{N} A_{jk}^{SI} P_k = \sum_{k=1}^{N} (A_{jk} + R_{jk}) P_k = E_{inc,j} \tag{21}$$

where the $A_{jk}$ term indicate the direct dipole-dipole interaction and is explained in free-space DDA (Eq.9) and $R_{jk}$ is the contribution from the reflected dipole interaction (Figure 9). The reflected component is solved in terms of Somerfield integrals. Since the spherical wave from each dipole is partially reflected and not equally in all

directions, a spherical wave can be decomposed into cylindrical and planar components [51] as depicted in Figure 10. The cylindrical wave will be unperturbed because it expands parallel to the surface. On the other hand, the planar wave propagates in direction normal to the surface and is partially reflected. The fraction of the reflected field strength is calculated using the Fresnel coefficients for the TE (transverse Electric) and TM (transverse magnetic) incident fields.

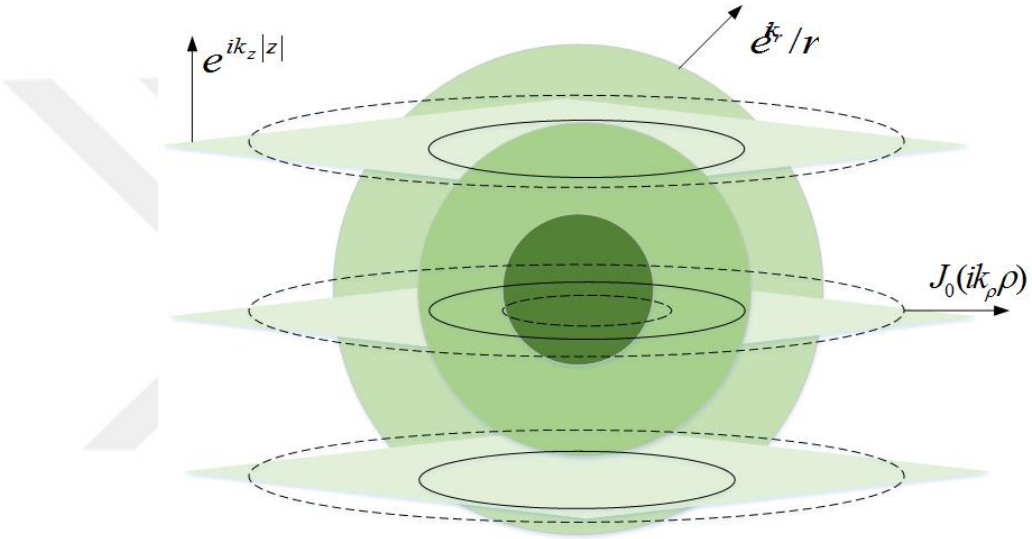


**Figure 10:** The spherical wave decomposed into cylindrical and planar components [2].

The following Somerfield integral is used to evaluate the Green's function of the electric field from a reflected dipole [51]:

$$\left(\frac{e^{ikr}}{4\pi r}\right)_{TE,TM} = \frac{i}{4\pi}\int_0^\infty \frac{k_\rho}{k_z} J_0(k_\rho\rho) R^{TE,TM} e^{ik_2(z_j+j)} dk_\rho \tag{22}$$

Where $J_0$, is the Bessel function and it represents the cylindrical wave component of the expansion whereas $e^{ik_2z(z_j+j)}$ is the planar component. By using the variable substitution, the integral is separated in to components that are evaluated using numerical integration [2].

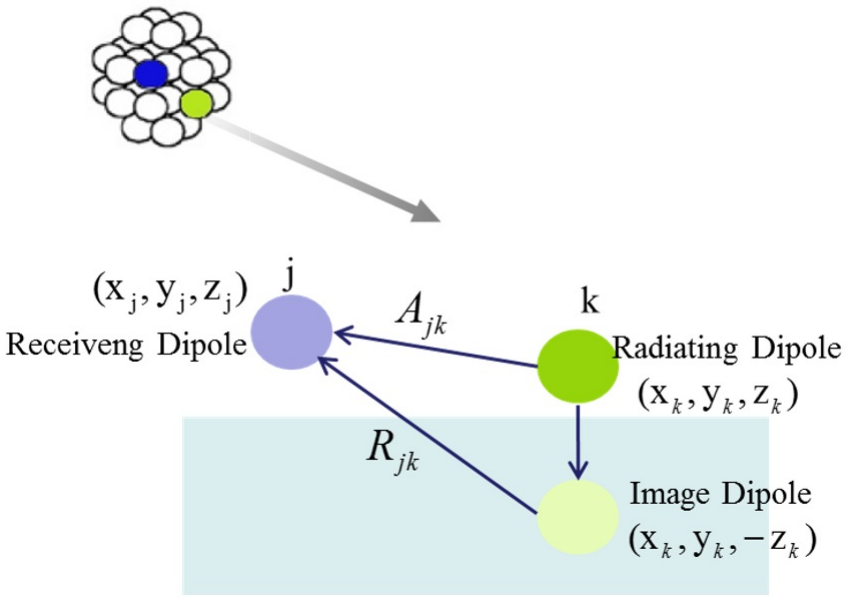


**Figure 11:** Radiating dipole over a surface, its image and the receiving dipole on the surface.

## *2.10 Scattered E-field in the Far-field Zone*

As mentioned in the previous section, the scattered EM wave in the upper half-space is the sum of the EM wave contributions as a result of the dipole moments of every dipole due to the interaction from the dipole-dipole and image (reflected) dipoles interactions. In the scenario where the source of EM wave is on the opposite side of the planar interface, there is no reflected component. However, the case of the incident plane wave undergoing total internal refraction because an evanescent field will exist along the media interface the formalism is discussed in Loke and Menguc [2] as shown in Figure 12 the scattered EM wave is calculated [38] using:

$$E_{sca}(r) = k_0^2 \frac{e^{ik_0 r}}{4\pi r} \sum_{j=1}^{N} \{e^{-ik_{sca}.r_j}[(p_j.\widehat{e}_1)\widehat{e}_1+(p_j.\widehat{e}_2)\widehat{e}_2]+e^{-ik_{sca}.r_j}[R^{TM}(p_j.\widehat{e}_1)\widehat{e}_1+R^{TE}(p_j.\widehat{e}_2)\widehat{e}_2]\} \tag{23}$$

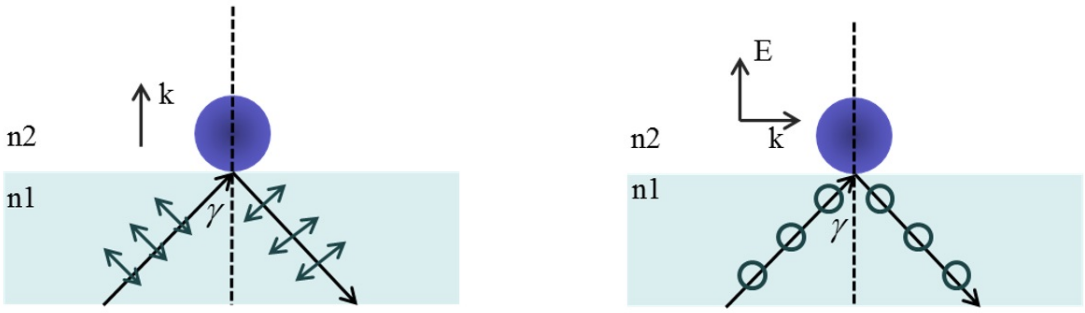


**Figure 12:** Total internal reflection of incident(a) TM and (b) TE plane waves from below the substrate surface. Evanescent waves exists above the surface.

where $\hat{e_1}$ and $\hat{e_2}$ are the unit vectors in Cartesian expressions of the $\hat{e}_\theta$ and $\hat{e}_\phi$ vectors in spherical coordinates, respectively, in the scattering frame (Figure 12). The radial component of the scattered field approaches zero in the far field. The reflected terms in Eq.21 are subject to the Fresnel reflection coefficients, $R^{TM}$ and $R^{TE}$.

## *2.11 Steps of DDA-SI calculations*

For clarity, the steps of calculation for the moment of particle on the substrate using the DDA-SI are summarized below [2].

*a*) Discretize the object into $N$ polarizable dipoles with effective radius $a_{eff}$ and create the coordinates for dipoles $r$.

*b*) Assign a refractive index $m$.

*c*) Calculate the electric field $E_{inc,j}$ at each dipole.

*d*) Calculate the polarizability $\alpha_j$ of each dipole.

*e*) Calculate the total interaction matrix $T$.

*f*) Choose the suitable method to solve the linear equation and calculate the total moment of the system.

After applying the solving the linear equation to calculate moment $P$, other quantities such as the Poynting vector, extinction, absorption and scattered field, scattering cross sections, phase function, Mueller matrix etc. can be calculated.

# CHAPTER III

# ITERATIVE METHODS TO SOLVE THE LINEAR SYSTEM

The linear system of equations Eq.21 to be used in the solution scheme are given by: $\overline{T}.\overline{P} = \overline{E}_{inc}$ where $\overline{T}$ ($\overline{R} + \overline{A} = \overline{T}$ total interaction matrix, $\overline{R}$: dipole-reflected matrix, $\overline{A}$: dipole-dipole interaction) is a known complex-symmetric $3N \times 3N$ , $\overline{E}$ is total electric field is complex known $3N \times 1$ vector and $\overline{P}$ is complex $3N \times 1$ vector is an unknown vector.

In general, there are two methods to solve the linear equations $\overline{T}.\overline{P} = \overline{E}$: direct and iterative [52]. For the coefficient matrix $\overline{T}$ which it has dimension of $K \times K$, direct methods to solve the linear equation require more computational effort proportional to $O(K^3)$ (in the DDA-SI $K = 3N$ ), multiplications and storage of $O(K^2)$ numbers [53]. Furthermore, for the particles with dimensions comparable with the wavelength, the large numbers of dipoles is required in order to gain a satisfactory approximation. Accordingly, the direct solution to solve linear equation becomes intractable. The basics step of the DDA-SI calculations is employing the versatile iterative method to solve dense matrix rather than direct method because direct inversion of the matrix is not feasible for most problems due to the huge memory requirements. Hence, through the DDA history, mostly iterative methods have been employed.

## *3.1 Iterative Methods*

Iterative methods start with an initial guess $x_0$ to calculate the linear system $Ax = b$ and iteratively improve upon the initial guess, $x_1$, $x_2$,... until some predetermined criterion have been satisfied. Generally, the iterative operation stop when either the

related error in $Ax_i = b$ is below a convergence threshold or when an upper limit on the number of iterations has been achieved; whichever comes primly.

$$\begin{bmatrix} a_{11} & a_{12} & . & . & . & a_{1n} \\ a_{21} & a_{22} & . & . & . & a_{2n} \\ . & . & . & . & . & . \\ . & . & . & & & . \\ . & . & & . & & . \\ a_{n1} & a_{n2} & . & . & . & a_{nn} \end{bmatrix} \begin{bmatrix} x_1 \\ x_2 \\ . \\ . \\ . \\ x_n \end{bmatrix} = \begin{bmatrix} b_1 \\ b_2 \\ . \\ . \\ . \\ b_n \end{bmatrix} \tag{24}$$

The iterative process is stopped when:

$$r = \frac{\|Ax_n - E\|^2}{\|E\|^2} < \varepsilon \tag{25}$$

where $x_n$ is the $n$th estimate of the total EM wave given by the iterative method, and $\varepsilon$ is the desired accuracy. All the iterative solvers require two main steps of computations: vector inner products and matrix-vector products (MVPs). Since for a large number of dipoles the most time-consuming operation is the MVP, our calculation is dependent on the number of MVPs required by each iterative method to achieve $r$. In addition, depending on the iterative method, one or two MVPs are computed per iteration. Draine et al. [23] has used a complex conjugate gradient (CCG) method to solve the linear system of equations for a free space scattering features by using the Parallel Iterative Methods (PIM), Flatau et al [54] compared the efficiency of iterative methods in the DDA for nonmagnetic scatterers. Yurkin et al [55] investigated the dependency of the iterative solvers on the refractive index of NPs. Quasi-Minimal Residual Method (QMR) is one of the most efficient iterative methods have been implemented by Lumme and Rahola [56] for solving the system of linear equations in the DDA and Rahola claimed that QMR is a best method for DDA in comparison with BiCG, CGNR, CGS, BiCGSTAB [57]. In contrast, QMR method does often fail to converge in the calculation for noble metal with high imaginary part

in the refractive index. In order to find an optimum iterative solver, matrix properties in the linear system of equations need to be investigated.

In the DDA-SI linear system, the total interaction matrix $T$ is a symmetric, not positive definite matrix meaning that the real parts of all the eigenvalues are non positive and well-conditioned matrix. The condition number describes how sensitive the calculation to small perturbations is. The set of all eigenvalues of the matrix $A$, or in other words, the solutions to the characteristic equation:

$$\det(A - \lambda I) = 0 \tag{26}$$

where $\lambda$ is the number of eigenvalues and *det* refers to the determinant and $I$ is the identity matrix.

An infinite condition number implies that $A$ is singular. The determinant for singular matrices, which are the matrices with no inverse, is zero, meaning that at least one of the eigenvalues is zero. Systems with a small condition number are said to be *well-conditioned*, whereas for large condition numbers, the descriptor *ill-conditioned* is used. The smaller condition number is preferred. Although, for singular matrices, $det(A) = 0$, the relation $det(A) \approx 0$ is not an appropriate measure of condition.

The interaction matrix for Au nano-sphere is a well-conditioned for the entire visible light range even for 600-700 nm wavelength in which its refractive index has high imaginary part and the condition number does not go to infinite numbers by increasing the wavelength. In this section, we aimed to prove that LSQR is the appropriate iterative solver in the implementations to the light scattering problem by a homogeneous sphere for the DDA-SI calculation. Our purpose is finding a more accurate solution which can be applied for all kind of the NPs with different shapes and especially for noble metals with high imaginary part in the refractive index. Strictly, it requires to compare various iterative methods under the same true residual norm stopping criterion. In order to assess the algorithm, we used LSQR and the two common iterative solvers GMRES and QMR which are used in the previous

DDAs calculation in solving the linear system. For explanation, we calculated relative residual of a single 50 nm diameter Au nano-sphere placed on the BK7 substrate for the wavelength 632 and 700 nm (is shown at Figure 6 the imaginary part of refractive index is large for these wavelengths) when illuminated by a plane wave.

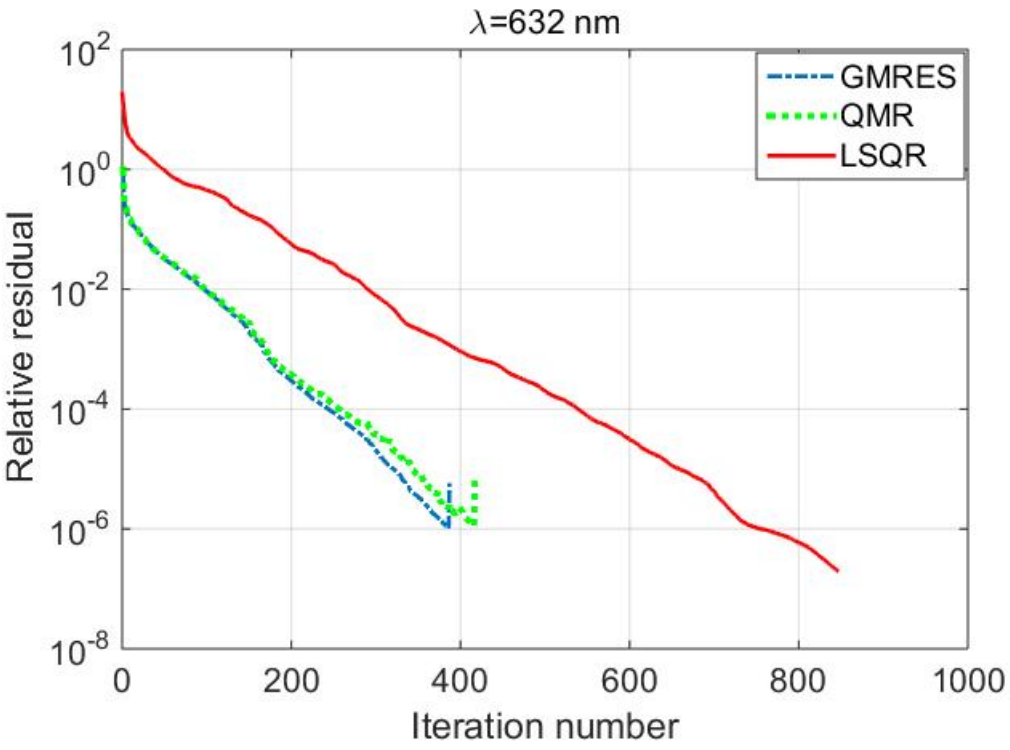


**Figure 13:** Relative residual for the 50 nm Au nano-sphere with dipole numbers $N = 552$ for three different iterative solvers when the wavelength is 632 nm.

The initial tolerance for the methods is set to be $10^{-6}$. As it is demonstrated in Figure 13 and 14, the LSQR method converged to the solution and other methods couldn't converge for the 632 nm and 700 nm wavelengths. Based on this analysis QMR and GMRES fail to achieve to the solution. However, for LSQR method convergence is achieved in the two mentioned wavelengths.

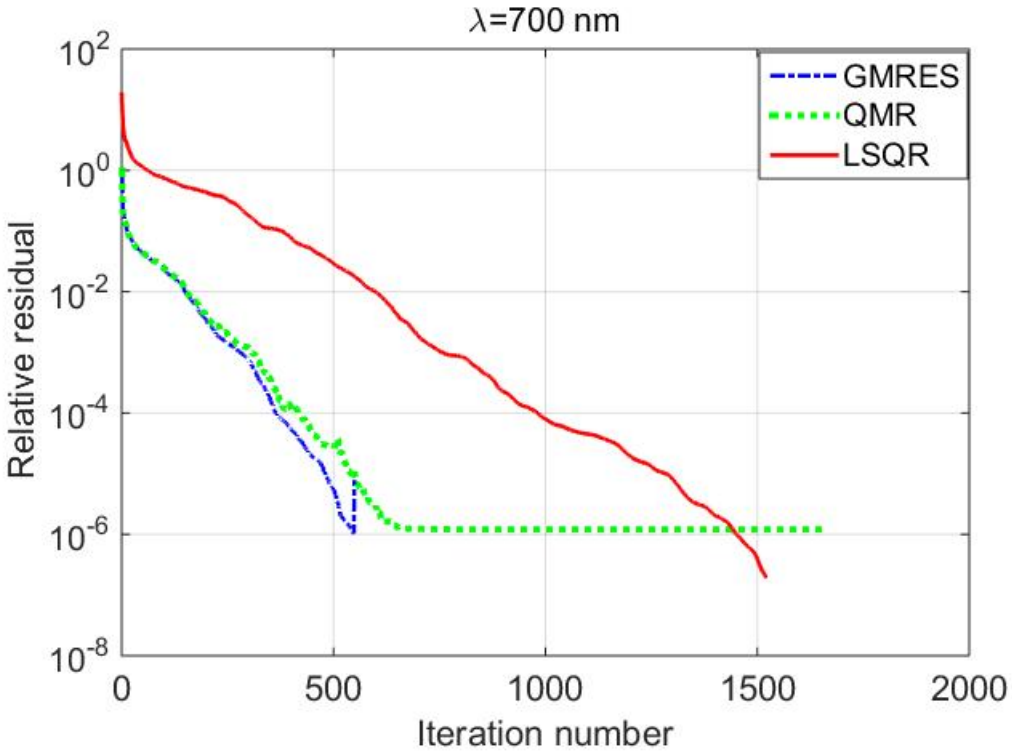


**Figure 14:** Relative residual for the 50 nm Au nano-sphere with dipole numbers $N = 552$ for three different iterative solver when the wavelength is 700 nm.

We extended the analysis by calculating the relative residual on the three methods in the entire visible wavelength. For fair comparison, we use the same setting which we applied to the maintained iterative methods. It is obvious from Figure 14, GMRES and QMR fails to achieve convergence; however, LSQR converges to the solution at the entire spectrum. Furthermore, as wavelength increased and the refractive index of Au becomes larger (Figure 6), GMRES and QMR methods fail to converge; however, it dose not have a detrimental effect on the convergence of the LSGR method.

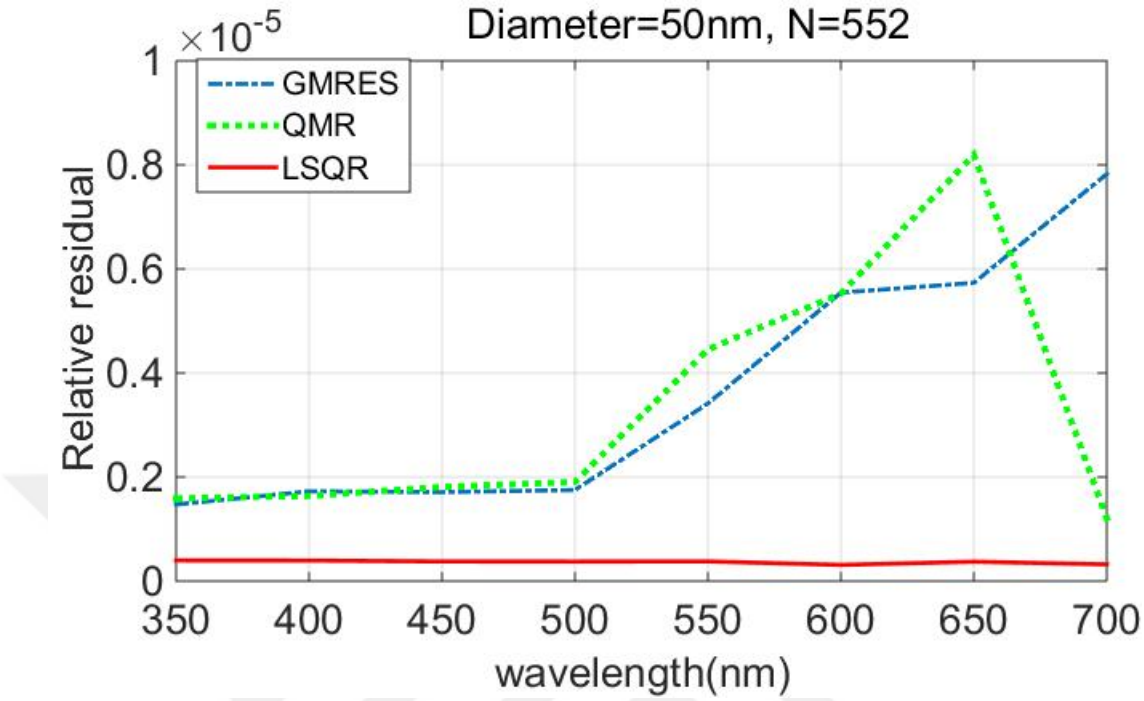


**Figure 15:** Comparison of the relative residual of the three iterative methods for single 50 nm Au nano-sphere on the BK7 substrate and 552 dipole number.

Moreover, based on Figure 15, the number of iteration for three iterative methods is increased by increasing the wavelength. We also analyzed the effect of size and dipole number by considering two different size of Au nano-sphere with diameters of 50 nm and 100 nm on the BK7 substrate. Again, for fair comparison, we set the tolerance to be $10^{-6}$ and studied the convergence of the LSQR method for the set of nano-sphere as dipole number 136, 280, 552 and 1472. It is clear from Figure 16.$a$ that LSQR achieve to convergence for the 50 nm Au nano-sphere in the different number of dipoles at the visible light range.

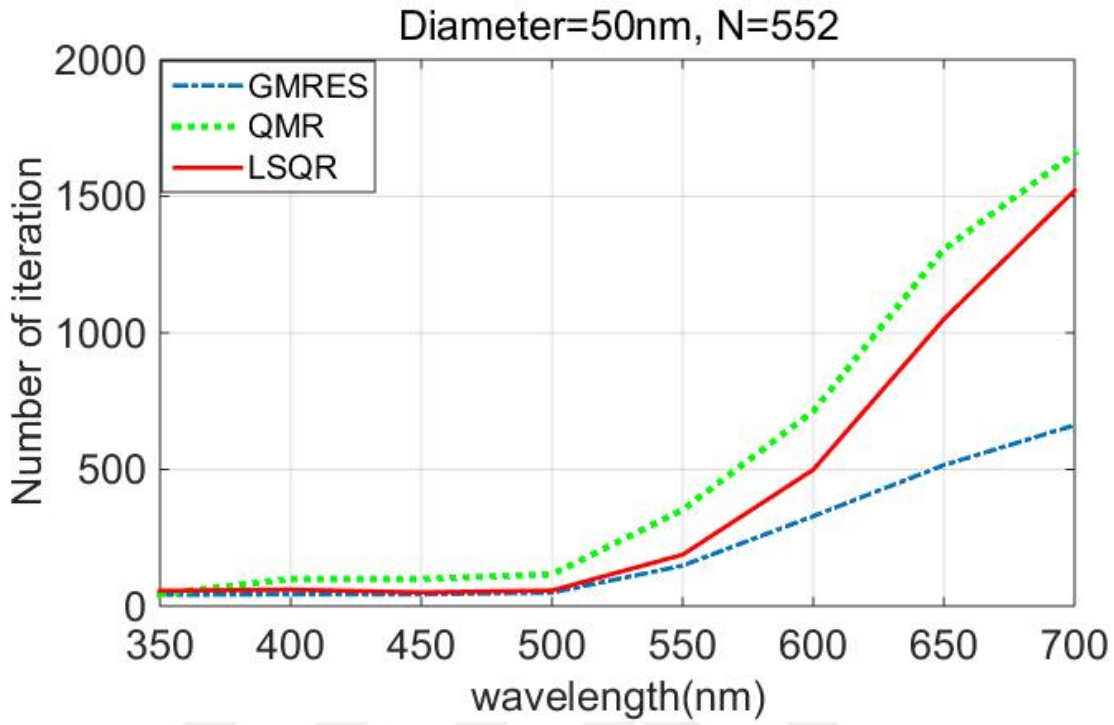


**Figure 16:** Iteration number of the GMRES, QMR and LSQR methods in the visible spectrum.

In addition, Figure 16.b shows that LSQR could converge for the larger diameter 100 nm of Au nano-sphere with different dipole number. On the other hand, based on the DDA-SI criteria, for noble metals ($d \leq 1/|m|k$), a large number of the dipoles is necessary in order to achieve a satisfactory approximation of the shape. Consequently, the converging to the solution with the specific tolerance could be achieved. As Figure 16 shows that the LSQR iterative solver converges for two different diameters (50nm and 100 nm) of a single Au nano-sphere on the BK7 substrate with relative residual $10^{-7}$ for different dipole numbers.

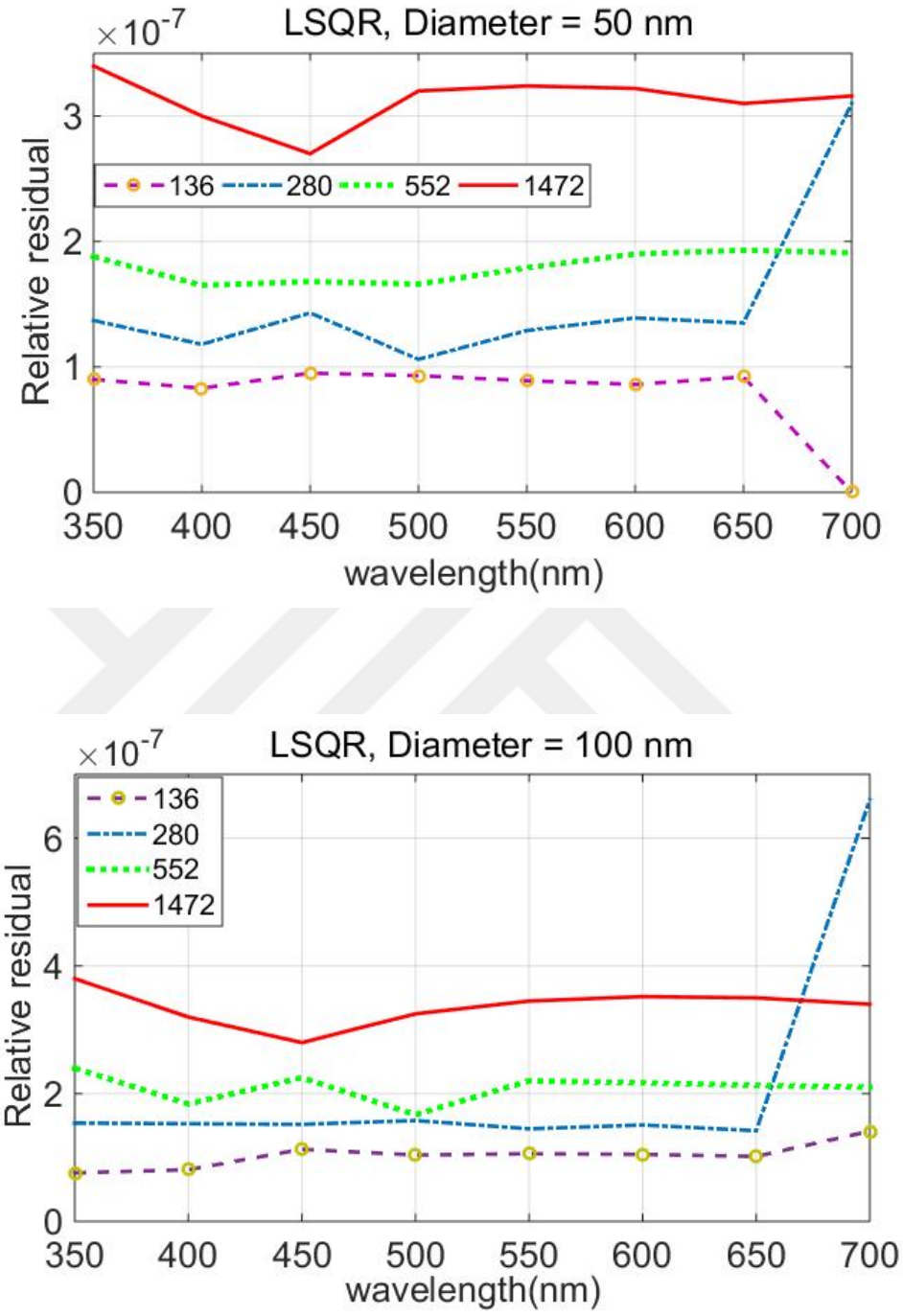


**Figure 17:** *a*) Relative residual of the 50 nm diameter Au nano-sphere on the BK7 substrate *b*) Relative residual of the 100 nm diameter Au nano-sphere on the BK7 substrate with dipole numbers=136, 280, 552 and 1472 in the visible light range computed by using the LSQR solver.

In this study, we aimed to decrease the iteration number of the LSQR solver to optimize the toolbox and make the calculation faster. In general, as mentioned in the previous section, the convergence of iterative methods in the DDA-SI calculation depends on the refractive index $m$ and by increasing the refractive index the convergence of iterative methods becomes challenging and most of the iterative solvers fails to converge in the calculation of the light scattering problem for noble metals. Furthermore, we demonstrated that the LSQR method converges and is the most versatile iterative method in the range of the spectrum where the imaginary part of the refractive index of Au is large. However; as the LSQR converges in relatively high number of iterations, using the preconditioning is devised.

## *3.2 Preconditioning*

Preconditioning method is a widely accepted method applied to many iterative solvers. The chosen preconditioner should be closely related to the original coefficient matrix and it attempts to reduce the condition number of the coefficient matrix $T$,improves the convergence of the associated linear system. However, this requires additional computational time during both initialization and each iteration. Preconditioning improves the convergence and speed it up in the linear system of equation $Ax = b$ by solving a similar system:

$$M^1 Ax = M^1 b \tag{27}$$

where the condition of $M^1 A$ is more appropriate than that of the primary matrix $A$; the matrix $M$ is the preconditioner matrix. LU-preconditioner (lower and upper triangle matrices) is one of the common preconditioners. They are produced by making a standard LU-decomposition of matrix $A$.

Based on the analysis of the matrix construction and its effect on number of iteration, we applied a Lower Upper (LU)-preconditioning to current DDA-SI coefficient matrix aiming for improving the convergence speed in the linear system of equations

[58]. We investigated the effect of using the LU-decomposition of the total interaction matrix $T$ as preconditioners to the iterative solvers.The preconditioning matrix is multiplied in each required step to finally calculate the estimated moment vector $P_k$ at the $k$th iteration step. Based on our results, we conclude that our method can significantly decrease the iteration numbers, thus making the toolbox faster.

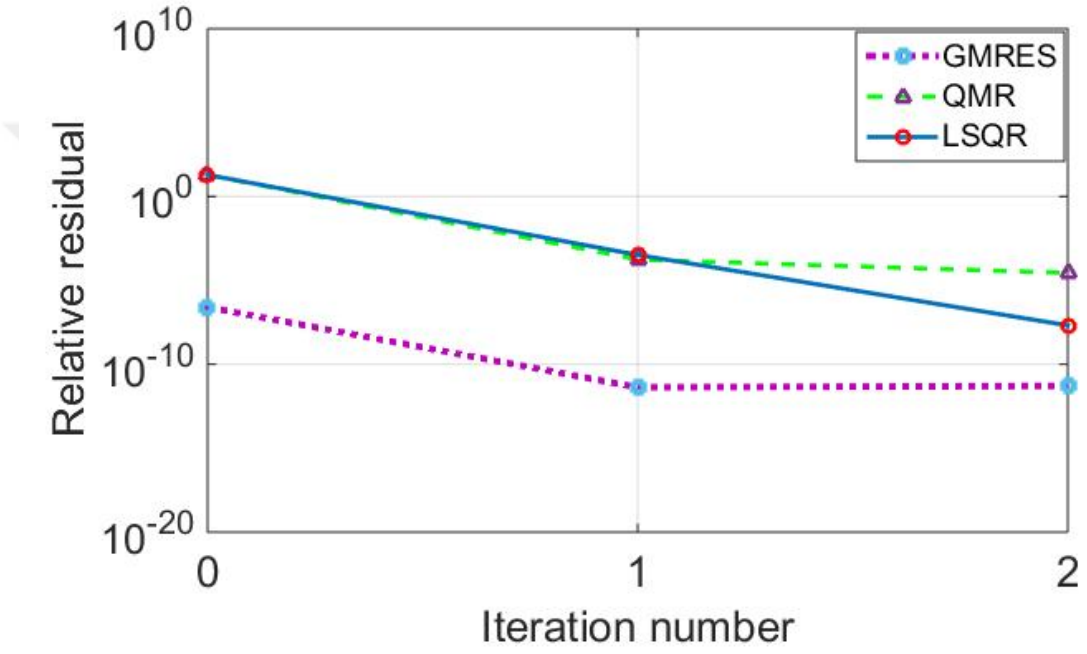


**Figure 18:** Comparison between convergence of QMR, GMRES and LSQR with LU-preconditioning.

We implemented and tested three different iterative methods GMRES, QMR and LSQR with and without LU-preconditioning when the prescribed tolerance is fixed to $10^{-6}$. The convergence of these methods are strongly depends on the refractive index of the NP. Figure 18 shows a comparison of the convergence rate for the three mentioned methods with LU-decomposition of the total interaction matrix $T$ as preconditioner. Based on the result, the QMR didn't converge and it is stagnated and

also the relative residual is stopped on $10^{-4}$. Furthermore, the GMRES solver stagnated and didn't converge to the solution although its initial tolerance is less than $10^{-6}$ the default tolerance value. However, the LSQR solver converged to the solution within 2 steps with relative residual on the order of $10^{-8}$. Therefore, the LSQR method is chosen to be a sufficient iterative method in the calculation of absorption efficiency of AuNP in the DDA-SI toolbox.

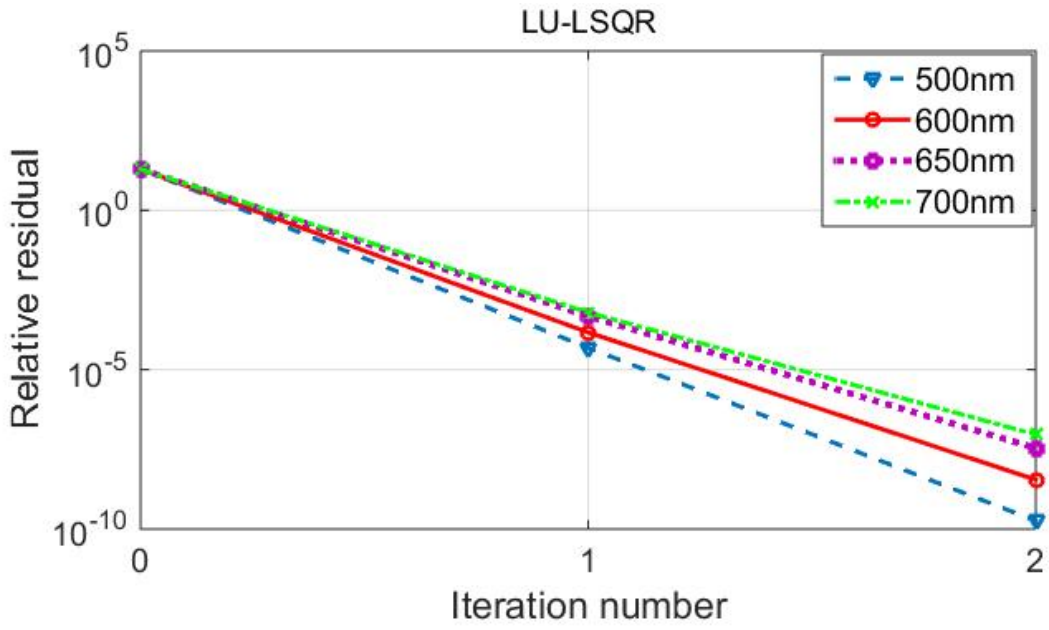


**Figure 19:** The calculation of relative residual for the Au nano-sphere with 50 nm diameter and dipole numbers = 552.

As mentioned before, in the plasmonic calculation using DDA-SI; the imaginary part of the refractive index for noble metals is large. Therefore, the condition number of the coefficient matrix for these particles becomes larger but does not go to infinity. The convergence ratio for 4 different wavelengths is depicted in the Figure 18 for single 50 nm AuNP on the BK7 substrate. It is clear that by increasing the wavelength the relative error is increased.

## *3.3 Calculation of Absorption Efficiency of Single Gold Nano-sphere*

In this section,the absorption efficiency (plasmon resonance) of single Au nano-sphere on the BK7 substrate where the EM wave is parallel and $k$ vector is perpendicular to substrate is analyzed by using the LU-LSQR solver. Figure 20 shows the absorption efficiency of 50 nm nano-sphere as a function of the number of dipoles in the visible light range spectrum. Based on this figure, the plasmon resonance for the single Au nano-sphere occurs at 515 nm. Moreover, there is a small artificial peak appeared between 590-700 nm wavelength associate with the low dipole numbers since by increasing the dipoles number, the peak is vanishing. Based on the results (Figure 20), the minimum dipoles number of $N$= 912 is required for proper analyzing of the single spherical NP on the BK7 substrate. It can be also concluded that after $N$= 912, the absorption efficiency barely changes by increasing the dipole number and the artificial peak disappears. The previous study of DDA formulations considered that the particle geometry is illustrated by set of the point dipoles. In order to achieve correct answer, high number of dipoles for the curvilinear and aspheric geometries is required.

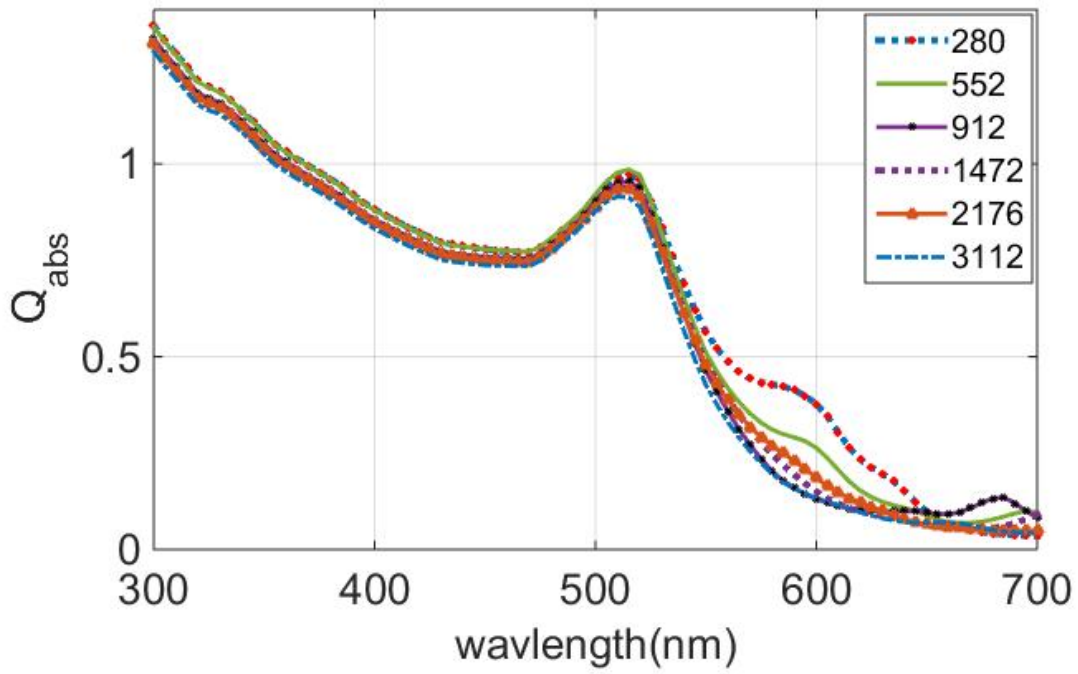


**Figure 20:** Change of absorption efficiency for a single 50 nm Au nano-sphere on the BK7 substrate.

Figure 21 is further analyzing the effect of the dipoles number on the absorption efficiency of the single Au nano-sphere on the BK7 substrate for various wavelengths. It is proving that there is a variation in the absorption efficiency for dipoles number less than 912 and the solution is barely changing by increasing the dipoles number for different wavelengths.

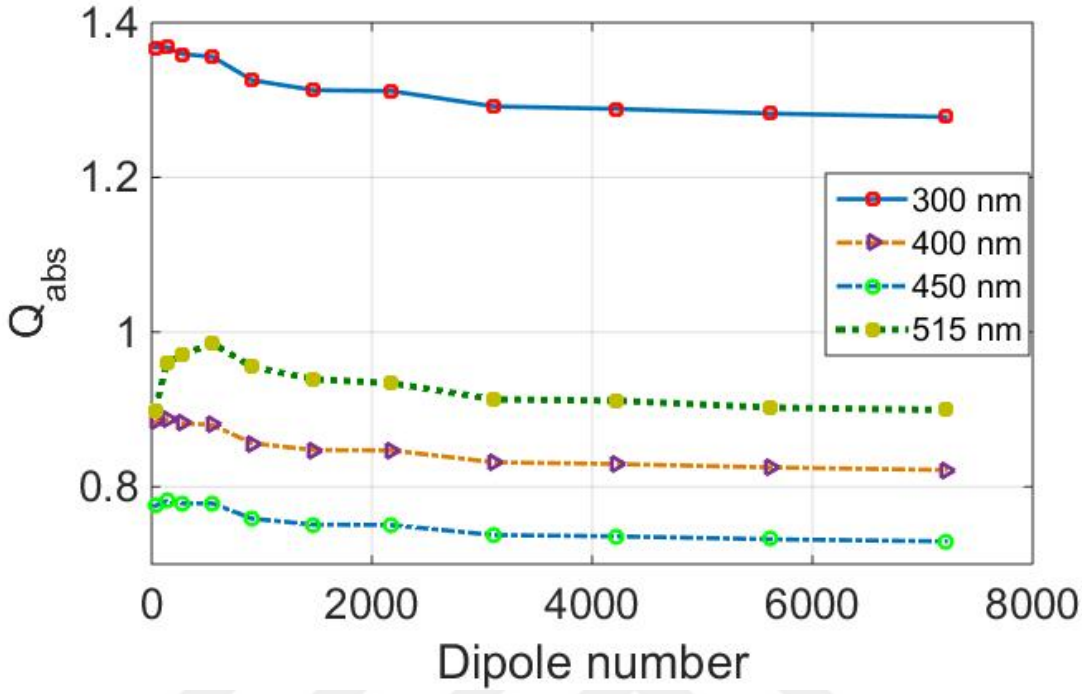


**Figure 21:** Absorption efficiency of 50 nm Au nano-sphere on the BK7 substrate versus number of dipoles $N$ for different incident wavelength.

## *3.4 Calculation of Absorption Efficiency of Single Gold Oblate Nano-sphere*

To obtain good and robust ascertainment about discretization criteria and the effect of the geometry on the plasmon resonance, we calculated the absorption efficiency of oblate spheroid AuNP in the BK7 substrate (Figure 22) as the same method in the case of the nano-sphere in the previous section. The Oblate spheroid particles like the sphere has a curvature geometry so the convergence happens in the larger number of dipoles. However; the curvature of the oblate spheroid is more than sphere, therefore, the correct answer is achieved in the larger number of dipoles than sphere. As it is shown in Figure 23 in order to adequate approximation, high number of dipoles is required.

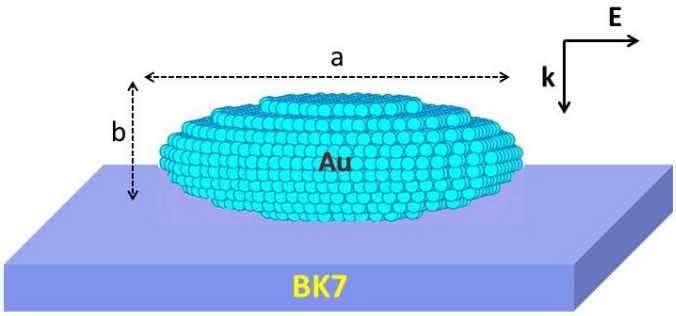


**Figure 22:** Schematic configuration of single oblate nano-sphere on the BK7 substrate

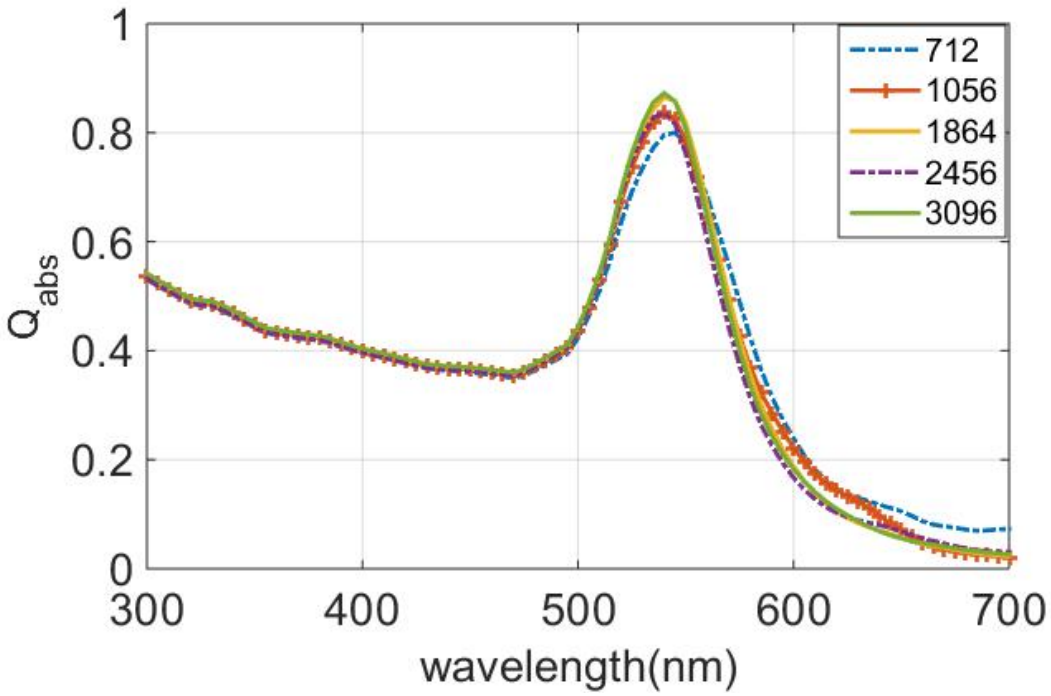


**Figure 23:** Change of absorption efficiency for a single 50 nm oblate spheroid AuNP on the BK7 substrate

In addition, as it is obvious in Figure 23, the increasing of the number of electrons per unit volume at the spheroid NP is caused to increase the electric filed enhancement close to the surface of the metal. Therefore, the plsmon resonance is red shifted to 540 nm in comparing with sphere. It is clear that there is a variation in the absorption

efficiency for dipoles number less than $N$=3096, therefore, the adulate dipole number for spheroid is $N$=3096.

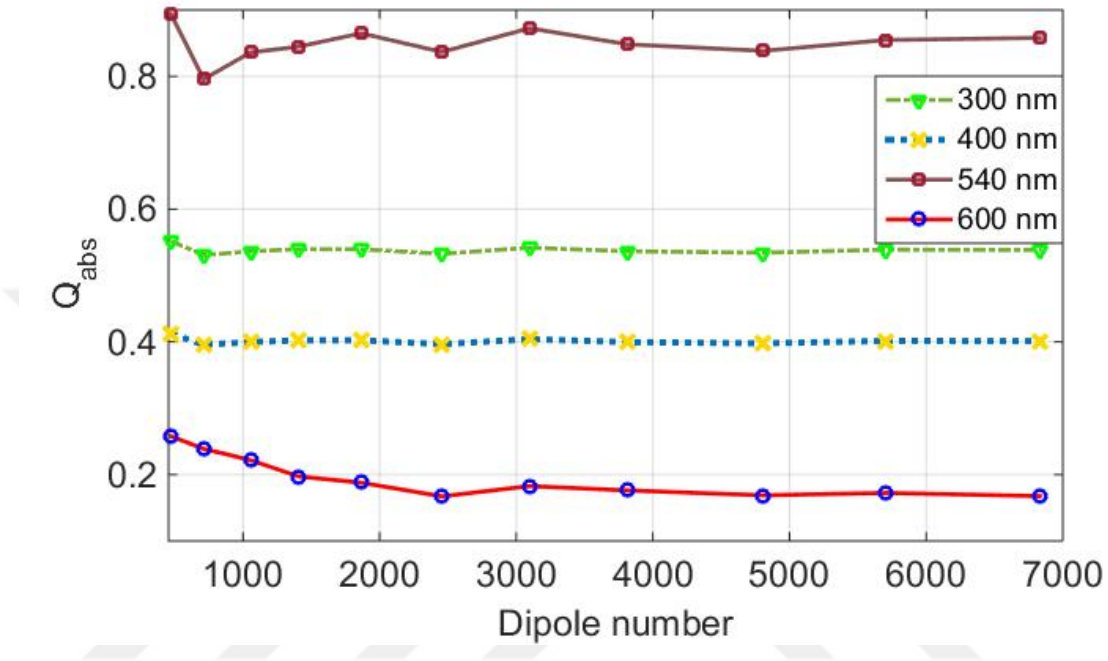


**Figure 24:** Absorption efficiency of 50 nm oblate spheroid AuNP on the BK7 substrate versus number of dipoles $N$ for different incident wavelength.

Figure 24 is further analyzing the effect of the dipoles number on the absorption efficiency of the single oblate spheroid AuNP on the BK7 substrate for various wavelengths. It is proving that there is a variation in the absorption efficiency for dipoles number less than $N$=3096 and the solution is barely changing by increasing the dipoles number for different wavelengths. In addition, for 540 nm wavelength which is the plasmon resonance for oblate spheroid AuNP, there is perturbation if $N < 3000$ numbers$< N$=3000. It is important to highlight that there are two main reason for this perturbation: large refractive index of AuNP for larger $\lambda > 500$ nm and curvature geometry of oblate nano-sphere.

## *3.5 Calculation of Absorption Efficiency of Single Gold Nano-cube*

Moreover, the absorption efficiency of a single 50 nm Au nano-cube placed on a BK7 glass has been shown in Figure 25 and Figure 26. We used the same method as in the case of nano-sphere to investigate the absorption efficiency of single nano-cube and the effect of dipoles number on it. In this analysis, effect of number of dipoles ranging from $N = 216$ to $N = 3375$ for 300 to 700 nm wavelength investigated. Figure 25 shows that the maximum absorption efficiency (plasmon resonance) of single Au nano-cube occurs at 525 nm. Furthermore,it changes by increasing the number of dipoles and after $N = 512$, the absorption efficiency and the plasmon resonance converge to its solution and further increasing the dipole numbers barely effects them. Cube unlike the sphere has a regular set of dipoles which well distributed thus, the proper discretization happens at lower number of dipoles in comparison with the nano-sphere and oblate spheroid case. This is due to the fact that high numbers of dipoles for adequately approximation of the curvilinear and spheric geometries are required in order to compensate for the *shape errors*. Therefore for our calculation the absorption efficiency of Au nano-cube, dipole number $N = 512$ is adequate approximation to achieve the correct answer.

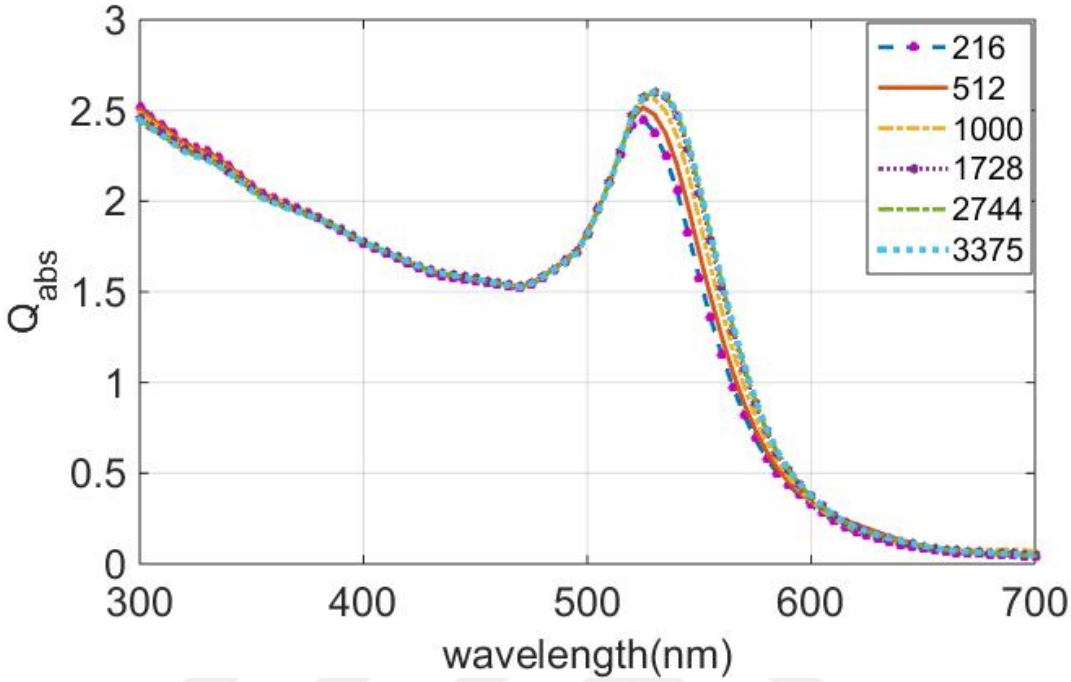


**Figure 25:** Change of absorption efficiency for a single 50 nm Au nano-cube as a function of wavelength for different number of dipoles.

Figure 26 is analyzing the effect of the dipoles number on the absorption efficiency of the single nano-cube on the BK7 substrate for different wavelengths. Similar to the nano-sphere case, the absorption efficiency of oblate nano-sphere for dipoles number more than 512 is barely changing by increasing the dipoles number.

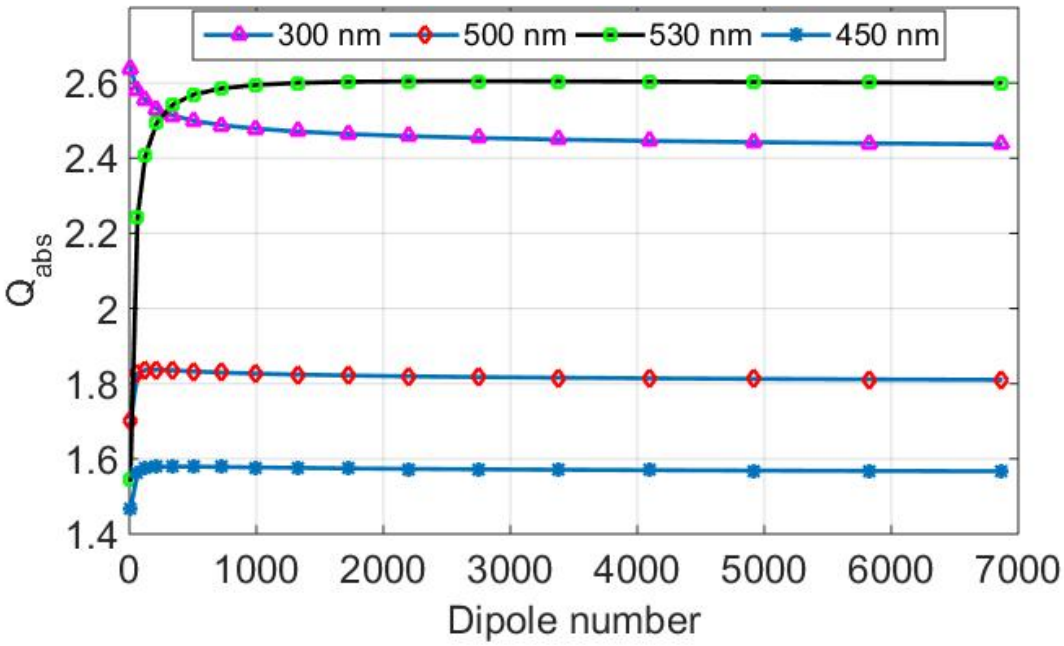


**Figure 26:** Absorption efficiency of 50 nm Au nano-cube on the BK7 substrate versus number of dipoles $N$ for different incident wavelengths.

## *3.6 Calculation of Absorption Efficiency of Single Gold Nano-pyramid*

Another important geometry of AuNPs used in the nano technology is pyramid. Nano-pyramid can be fabricated on different substrates like silicon (Si) or glass (BK7). They can be fabricated in different sizes and aspect ratios. In order to investigate the optical properties of these nanostructures, which is important for the mentioned applications, we calculate the absorption efficiency of single Au nano- pyramid placed on a BK7 glass (Figure 27). The base of nano-pyramid is square and each side of base is 100 nm and the apex is directly above the center of the base with the 50 nm hight.

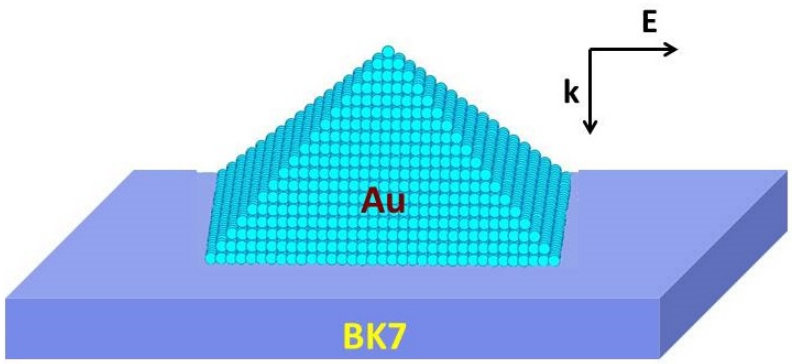


**Figure 27:** Schematic configuration of single nano-pyramid on the BK7 substrate illuminated by plane wave

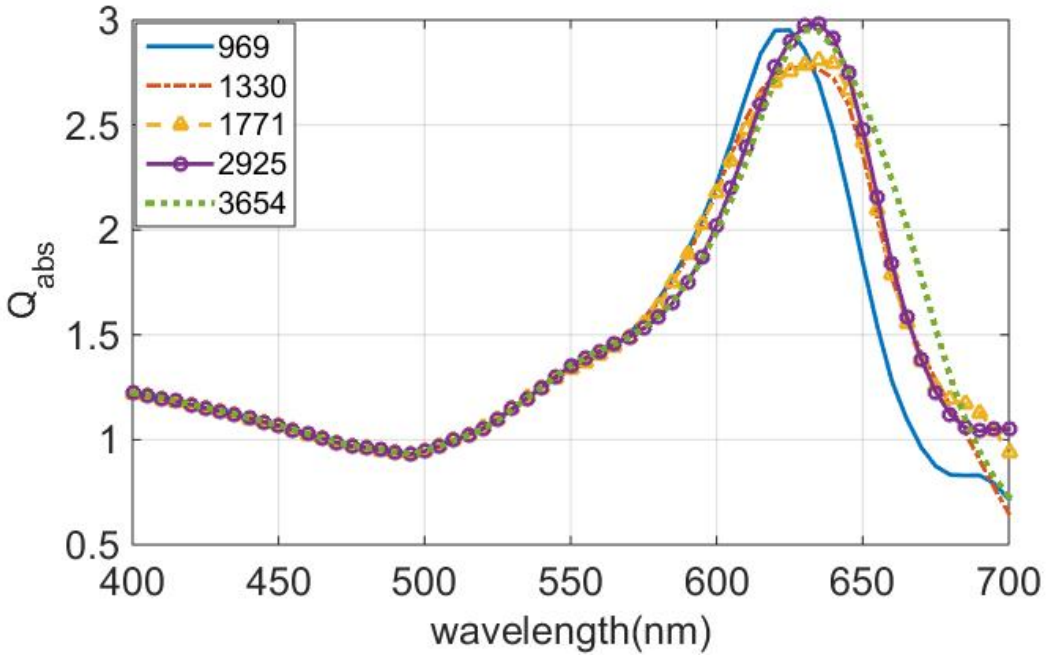


**Figure 28:** Change of absorption efficiency for a single 50 nm nano-pyramid on the BK7 substrate

We used the same method as in the case of the previous NPs in order to investigate the plasmon resonance and the effect of dipoles number on the Au nano-pyramid. Figure 28 shows the effect of number of dipoles ranging from $N = 969$ to $N = 3654$

for 300 to 700 nm wavelength. As it is clear that the maximum absorption efficiency (plasmon resonance) of single Au nano-pyramid occurs at 635 nm. Furthermore, it changes by increasing the number of dipoles and after $N = 2925$, the absorption efficiency and the plasmon resonance converge to its solution and further increasing the dipole numbers barely effects them.

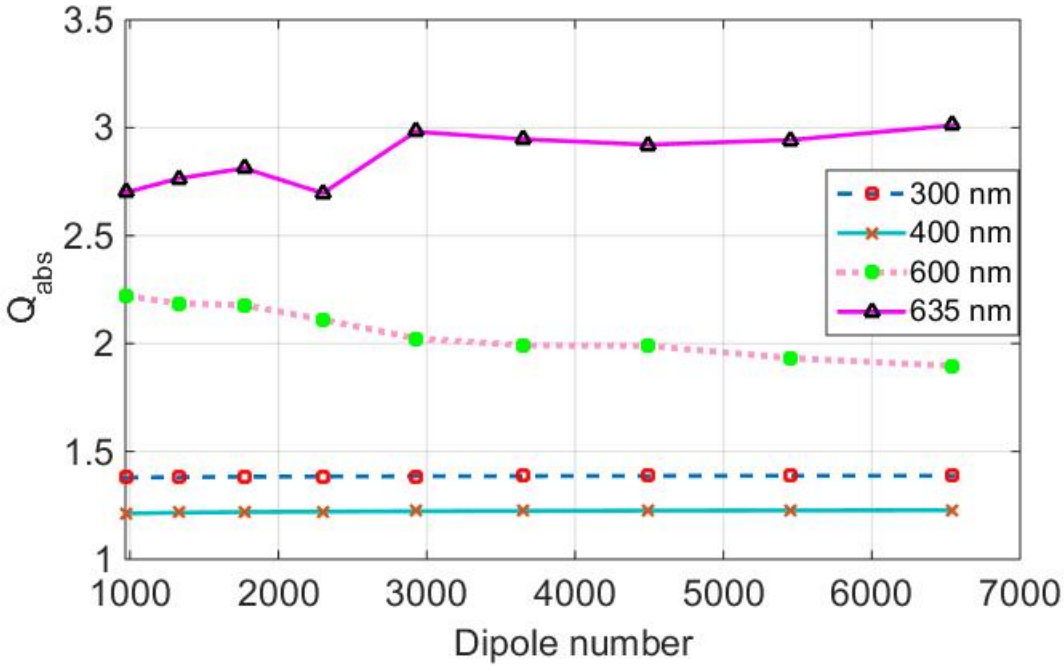


**Figure 29:** Change of absorption efficiency for a single 50 nm nano-pyramid on the BK7 substrate

Au nano-pyramid unlike the sphere and oblate spheroid has a regular set of dipoles which well distributed, however; the sharpness of the apex and high slope of pyramid could cause the perturbation in convergence for small number of dipoles.(Figure 29) Therefore, the proper discretization happens at higher number of dipoles in comparison with the previous cases. This is due to the fact that high numbers of dipoles for adequately approximation of the complex geometries are required in order to compensate for the shape error. We conclude that, for calculation the absorption efficiency

of Au nano-pyramid, dipole number $N = 2925$ is adequate approximation to achieve the correct answer.

## *3.7 Parallel Memory Allocation*

The parallel computing toolbox of MATLAB allows us to solve computationally intensive and data-intensive problems more quickly. It could run on our local multi core computer or on Shared Computing Cluster. Parallel processing operations such as parallel for-loops and message-passing functions let us implement task- and data-parallel algorithms in MATLAB. Converting serial MATLAB applications to parallel MATLAB applications generally requires few code modifications and no programming in a low-level language is necessary. We can run our parallel applications interactively or in batch mode by using $parfor$ function in MATLAB.

## *3.8 Validation with Previous Toolbox*

For confidence, we compare the absorption efficiency of single Au nano-sphere on a BK7 glass substrate undergoing TE evanescent field illumination (Figure 12) where comparisons are made between DDA-SI-3 and Moghadam et al [3]. The number of dipoles used for the DDA-SI simulations was $N = 912$. It can be observed in Figure 30 that there is an exact agreement between two toolboxes.

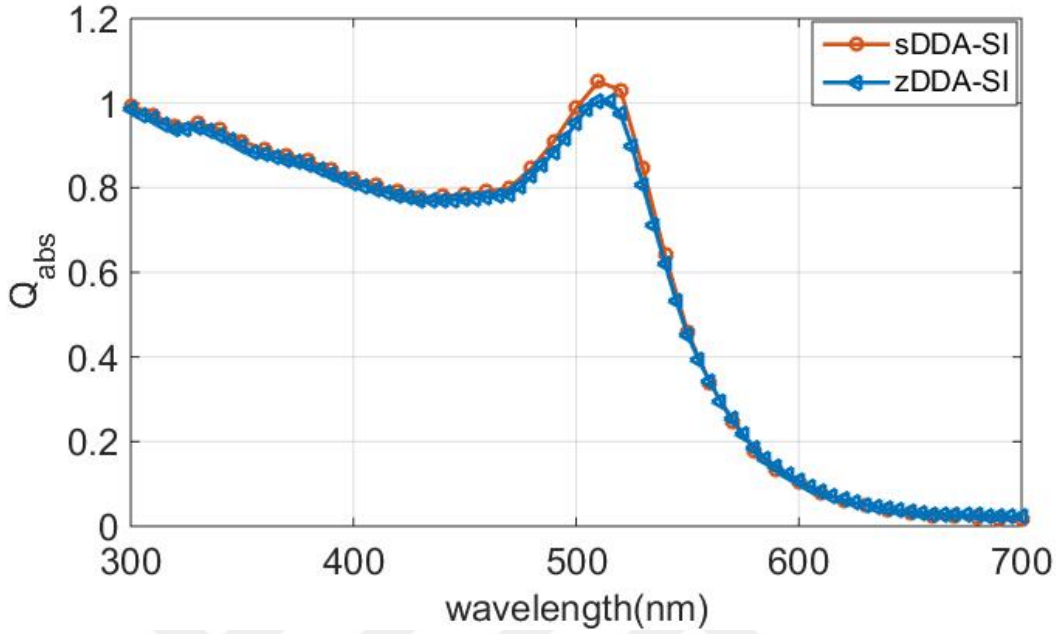


**Figure 30:** Comparison of absorption efficiency of single Au nano-sphere illuminated by evanescence wave calculating with two toolbox (Moghaddam et al [3] and this thesis)

## *3.9 Vectorized DDA-SI Toolbox*

The DDA-SI offers a further improvement integrating the surface interaction by an analytical formulation. For dimer and trimer investigation on the substrate, due to the dipole-dipole interaction, surface interaction and the large number of dipoles to be accurately approximation, computational time demand would be significant. We used three toolboxes of original one by Loke et al [4]., vectorized toolbox by Moghaddam et [3], and our optimized toolbox which contains the vectorization and optimazation the iterative solver of linear equation to calculate the absorption efficiency of a single Au nano-cube on a BK7 substrate illuminated by a plane wave at 600 nm wavelength. The properties of DDA-SI toolboxes is shown in the Table 3. We used a computer with Intel(R) core(TM) i7, 4770 @ 3.40 GHz CPU and 24 GB RAM capacity running

on 64 bit windows 7 operating system.

**Table 3:** Three DDA-SI Toolboxes

| Name | Developted by | Solving method | Properties | Convergence |
|---|---|---|---|---|
| $DDA-SI-$ [22] | V. Loke & M.P. Menguc | GMRES & QMR & MINRES | *for* loops | Not converged for AuNPs for large refractive index |
| $DDA-SI-2$ [32 ] | S. Moghaddam , H. Erturk& M.P. Menguc | Single vs. Double,Precision GMRES & BICG & ... | vectorized | Not converged for AuNPs for large refractive index |
| $DDA-SI-3$ [55 ] | Z.R. Fathi & M.P. Menguc | LU-LSQR | vectorized | Converged for AuNPs for |

The iterative solver used in two other toolbox was GMRES and we compared the performance with the proposed method of using LU-LSQR iterative solver. Figure 31 demonstrate that our proposed method is the best among the two mentioned toolboxes in the case of solving time. It is also proved that although the LU-decomposition is an extra step in the calculation and requires more time to be calculated, using the LU decomposition of the coefficient matrix as the preconditioner for LSQR solver speeds up the calculation by decreasing the iteration numbers to two steps; consequently, the overall performance became roughly 4.5 times faster than the previous version of the toolbox.

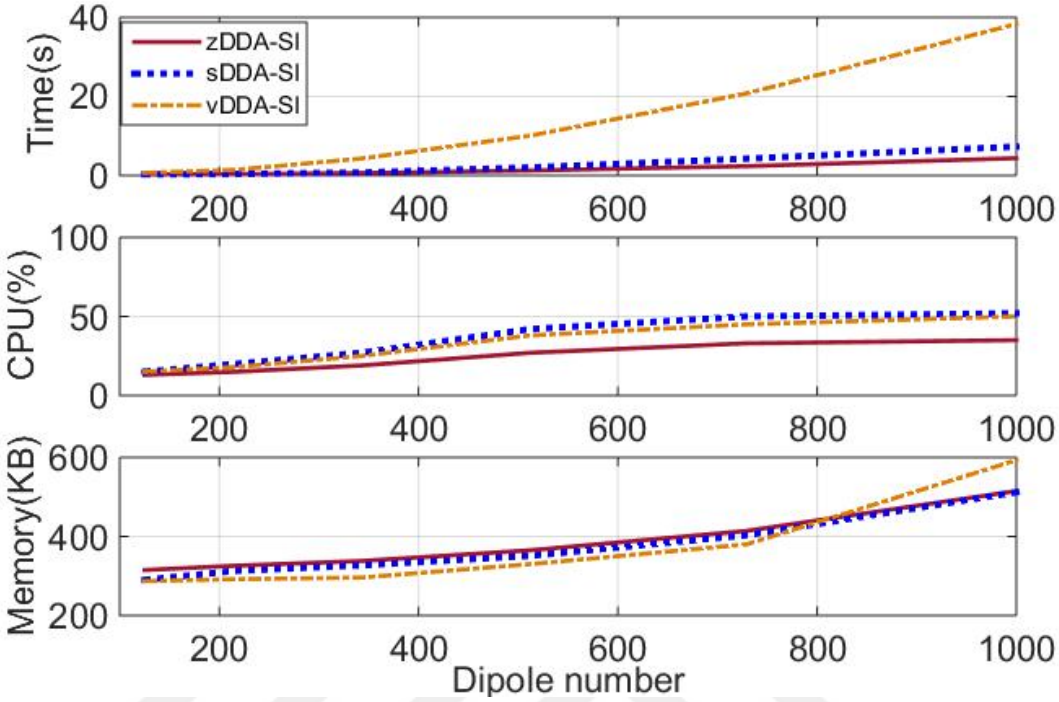


**Figure 31:** Comparison of three DDA-SI toolboxes, zDDA-SI(this thesis method), Moghaddam et al(sDDA-SI) [3] and Loke et al(vDDA-SI) [4].

In this thesis and also Moghaddam et al [3] vectorized DDA-SI functions in order to improve and speed up the performance of the toolbox. The process is done to revise the loop-based codes by using MATLAB matrix and the vector in the main DDA-SI toolbox is used. Figure 31 proves the time difference between three types of problems and it can be seen that vectorization helps in speeding up the calculation.

# CHAPTER IV

# COMPARISON DDA-SI AND FEM METHODS

In this Chapter we investigated the plasmonic response of Au nano-cubes on the BK7 substrate is done using DDA-SI and the results are bench marked with results of finite-element methods (FEM) [59]. We benchmarked the DDA-SI MATLAB toolbox against the FEM for the accuracy when modeling surface plasmon resonance of one Au nano-cube on the BK7 substrate, without any volume correction. Errors are eliminated in the DDA-SI implementation where the particle sits on a substrate involves illuminated by a plane wave [30].

The finite-element method (FEM) involves solving the Helmholtz equation where the spatial derivatives at the surface of the object are solved numerically as a boundary condition problem. FEM can be used to simulate the light scattering from arbitrarily shaped, inhomogeneous and anisotropic structures for a single frequency at a time. An appropriate grid mesh or element (triangular, tetrahedral or hexahedral) is used to illustrate the surface or structure. The mesh can be denser to represent regions with fine structure. For heating of noble metals on substrate, Huda et al [59]. investigated the effect of using Au nano-sphere and Si tapping mode AFM tip with FEM.

The steady spatial distribution of $E$ and $H$ at the node points is the quantities of interest. In the FEM, the linear system can be solved by using Gaussian elimination or the conjugate gradient method. The coefficient matrix for the system of equations represents only the interactions between neighboring grids mesh cells and thus will be a banded diagonal. The recommended mesh cell size is, though in some cases $\lambda/5$ has been proven is sufficient.

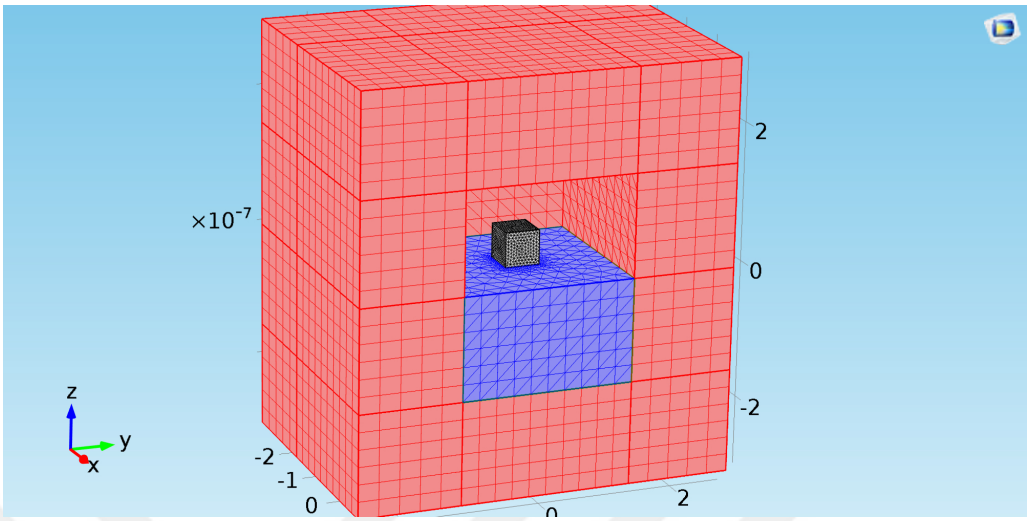


**Figure 32:** Meshed representation of simulation medium in COMSOL. The PML is recognized in red and the substrate is in blue color.

The calculation region for the FEM is larger than the object itself. The Helmholtz equation is an elliptic differential equation that is solved as a boundary value problem at the surface and at the edge of computational domain (simulating infinity).

## *4.1 FEM Simulation for Single Nano-cube on the BK7 Substrate*

For the simulations, we used RF module of COMSOL Multiphysics ® 5 which calculates the difference between a volume source field defined in the absence of a scatterer and the total field in the presence of the scatterer. This difference is referred to as the scattered field, which still provides access to the details of the near field and should not be confused with techniques for calculating the scattered far field. We defined the source field as a plane wave of wavelength between 400 and 700 nm. The source field was defined analytically, using the Fresnel equations over the entire 3D simulation domain, excluding the perfectly matched layers (PML), as if the NP was absent. For TE simulations the source field was specified in terms of $E_z$, while for TM simulations the source field was specified by $E_x$ and $E_y$. Tetrahedral elements

are used to model the structures. The simulation domain is surrounded by the PML absorbing boundary.

-

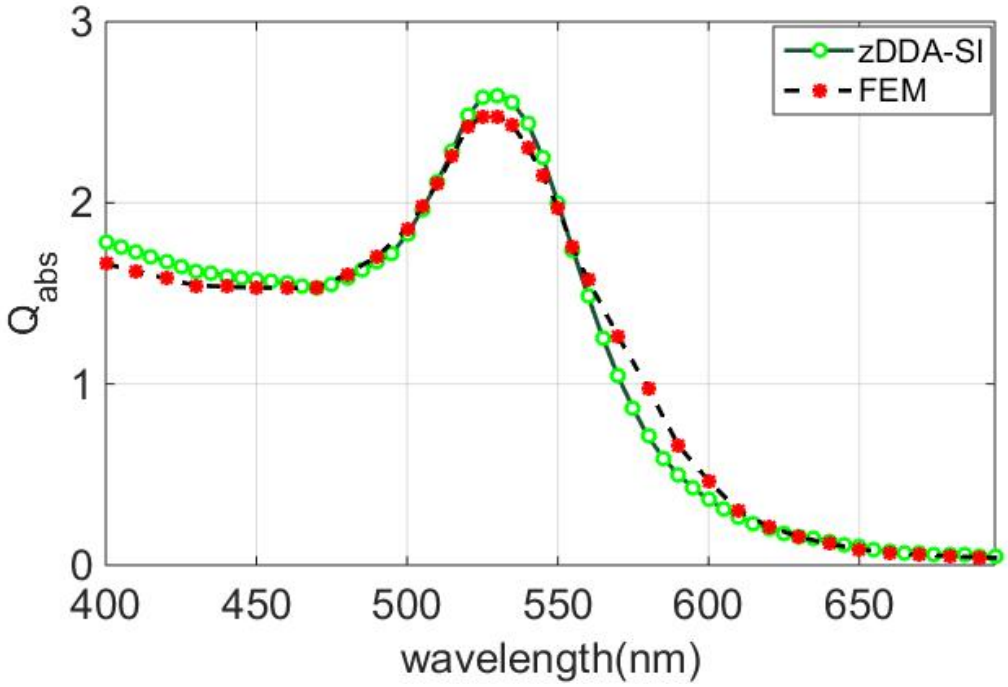


**Figure 33:** Comparing of DDA-SI and FEM methods for absorption efficiency spectra of the 50 nm cube on a BK7 glass planar substrate, illuminated by a plane wave propagating surface $N_C = 343$.

Additionally, scattering boundary conditions are defined at the outer boundaries. Figure 32 is the mesh representation of simulation medium. The PML is recognized in red color and the substrate is in blue color. We meshed the cubic NP and substrate with the Free Tetrahedral method and it has 33601 mesh elements for the NP and 6471 mesh elements for the substrate.

## 4.2 COMSOL Implementation for FEM Calculations

There are two ways of implementation of RF scattering problems in FEM [60]; solving for scattering field or solving for total field. There are some advantages and disadvantages in both cases depending on what you want to calculate, how much memory is available and some FEM issues, one of the approaches could be selected [59].

This thesis uses solving for total field or two steps approach. In this method, first NP is considered as air and electric field is calculated in the domain. For this, two ports boundary condition is used. The transmitting port is placed above the substrate and exciting the plane wave and another port is placed at the bottom of substrate to absorb all the receiving energy. Also Perfectly Matched Layer (PML) is needed to collect the reflected waves coming from substrate and not letting it inter back to the simulation medium. After finding the solution, it is fed back to the simulator as an excitation or initial value for the case that NP is considered. Note that in order to get correct results, in material properties of NP and substrate, the complex refractive index of both NP and the substrate should be used. COMSOL by itself does not feature this properties and one should import these properties as a frequency dependent functions which further will be used by simulator. In order to find the absorption efficiency of scatterer, the volume integral of the dissipated power should be taken over the NPs. In order to be sure that the result has enough accuracy, NPs should mesh very fine and dense. Also in order to avoid reflection from PML, its thickness should be at least twice the biggest wavelength. The mesh size should be at least ten time smaller than the smallest wavelength in order to calculate with adequate accuracy.

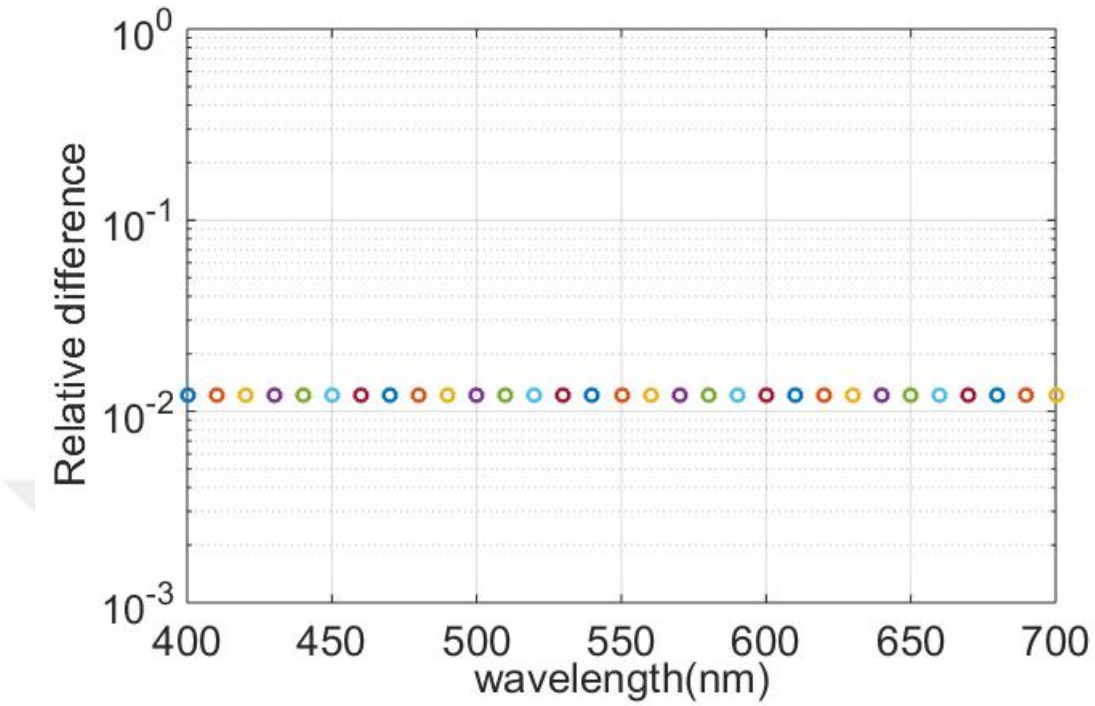


**Figure 34:** Relative difference between FEM and optimized LSQR version of the DDA-SI for absorption efficiency of one Au cube on the BK7 substrate.

Figure 33 and Figure 34 representing the comparison between DDA-SI results and COMSOL. From these pictures it is clear that the implemented methods in solving linear equation in our DDA-SI toolbox is accurate enough in which the relative error between solutions of DDA-SI and FEM is on the order of 0.01 or 1% over 400 nm-700 nm spectrum.

# CHAPTER V

# PLASMON RESONANCE OF DIMER AND TRIMER OF GOLD NANO-PARTICLES

In this section, we numerically investigated that due to coupling of AuNPs in dimers and trimers, the large spectral shifts of plasmon resonance modes is created. These simulations of the plasmon response of Au nano dimers and trimers on BK7 substrate have been performed by running DDA-SI on an Intel 16 Core 3.48 GHz CPU with 24 GB RAM. In order to find a correlation between the geometry and the plasmonic resonances, we calculate the absorption efficiency of the number of nano-structures including dimers (two AuNP), trimers(three AuNP) which formed by cubes, spheroid (sphere and oblate spheroid ) and pyramid.

## *5.1 Plasmon Resonance of Spherical Gold Particles*

In order to obtain comprehensive knowledge of plasmon modes due to the tuning the geometry and gap separation between AuNPs, we calculated the interaction of spherical dimers and trimers of spherical AuNPs.

### 5.1.1 Dimer of gold nano-sphere in the different distances

In the chapter III, we calculated the absorption efficiency of 50 nm single AU nano-sphere in the BK7 substrate. Furthermore, we showed the plasmon resonance of nano-sphere AuNP is around 515 nm. In this section, the absorption efficiency of 50 nm Au nano-dimer formed by two nano-sphere with the same diameters placed on a BK7 glass for the plane wave is calculated as is depicted in Figure 35. The electric field is parallel and $k$ vector is perpendicular to substrate. This is similar to analysis discussed by Ivezic et al. [61], which is related on dependent and independent

absorption regimes. The purpose is to observe the limits of dependent absorption exist for two particles when the distance $d$ between them is larger than three times the radius of a single sphere ($d > 3a$) where $a$ is the radius of the sphere and $d$ is the distance between the NPs.

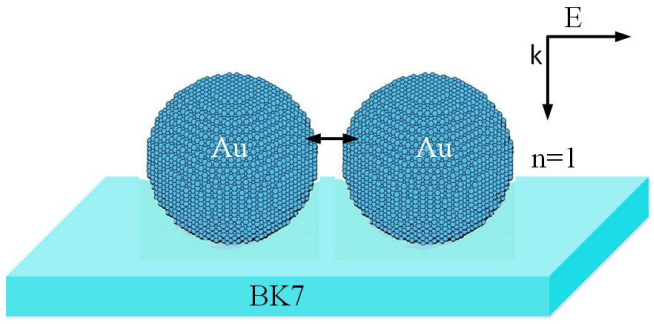


**Figure 35:** Illustration of the Au spherical nano-trimer on the BK7 substrate with six different spacing.

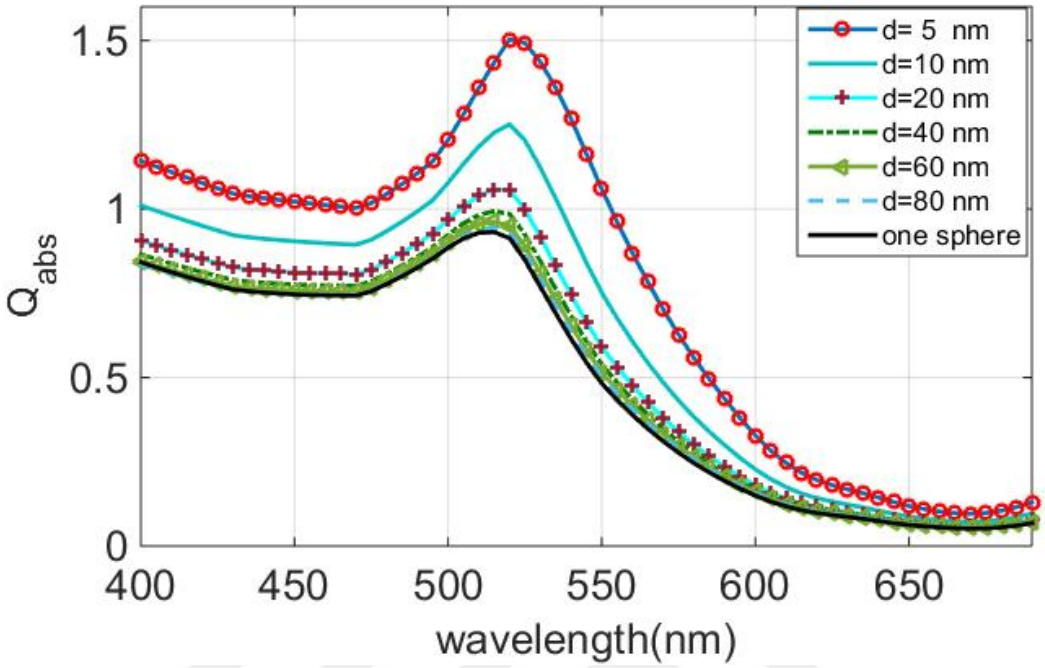


**Figure 36:** Absorption efficiency of 50 nm Au spherical dimer on BK7 substrate with different distances.

As it is shown in Figure 36, changing the distance between AuNPs of spherical dimer will results in changing the absorption efficiency and it has no influence in resonance frequency.

### 5.1.2 Trimer of gold nano-sphere

In order to better understand of the inter coupling between nano-spheres, we investigated the plasmon resonance of three nano-spheres. The schematic graph of the Au nano-trimer nanostructure is plotted in Figure 37. In this Figure all of the nano-spheres have the same volume (Diameter=50 nm) and the gap distance is 5 nm. Figure 38 shows that by increasing the number of nano-spheres when the distance of nano-spheres is 5 nm in both dimer and trimer, the absorption efficiency increases and red-shift happens in the resonance frequencies.

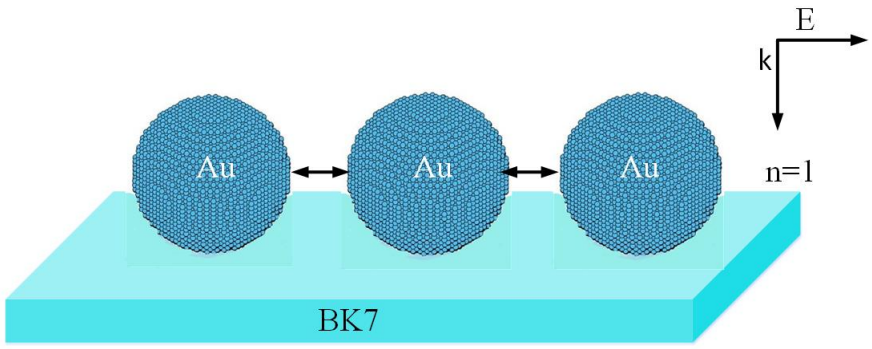


**Figure 37:** Illustration of the Au spherical trimer NPs on the BK7 substrate with 5 nm spacing.

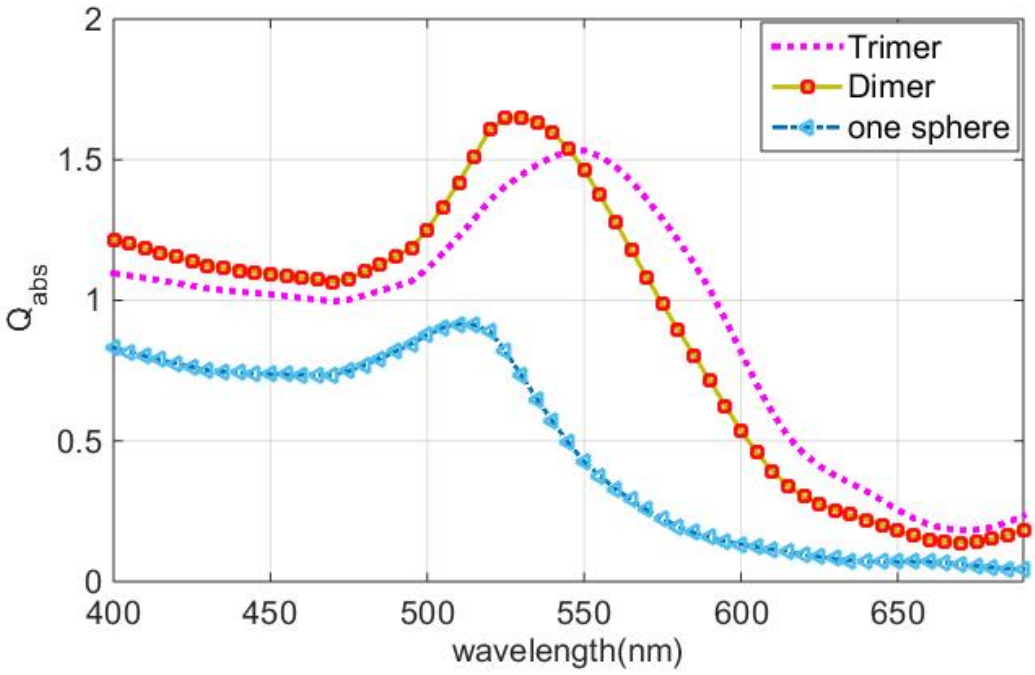


**Figure 38:** Absorption efficiency of 50 nm Au spherical dimer and trimer on BK7 substrate with 5 nm distances.

### 5.1.3 Dimer of gold spheres with different sizes

After investigating the effect of distance of Au nano-spheres dimer and trimer, the next step is to investigate what happens when the size of one of the spheres decreases compared to the other one as depicted in Figure 39. There are two restrictions about lattice spacing and dipole numbers for dimers and trimers. *a*) Since the lattice spacing influences on interaction matrix, the distance of dipoles (lattice spacing) must be equal for all particles because by varying the distance of dipoles the interaction between them changes.(interaction matrix is dependent on the distance of dipoles Eq.11) In this case the lattice spacing of all particles should follow the following relation:

$$d = \left(\frac{V_1}{N_1}\right)^{1/3} = \left(\frac{V_2}{N_2}\right)^{1/3} = \left(\frac{V_3}{N_3}\right)^{1/3} = ... \tag{28}$$

*b*) In the case of analyzing plasmon response of NPs with different sizes, the adequate dipole number for single NP whose size is the smallest should be chosen first and then according to the following equation, the dipole number for next bigger NP should be driven. For instance, the minimum dipole number for spherical NP giving correct answer is $N_s = 912$. It is worthwhile to mention that only in this case, the correct answer for dimer and trimer NP with different sizes is achievable.

$$N_2 = N_1 \left(\frac{V_2}{V_1}\right) \tag{29}$$

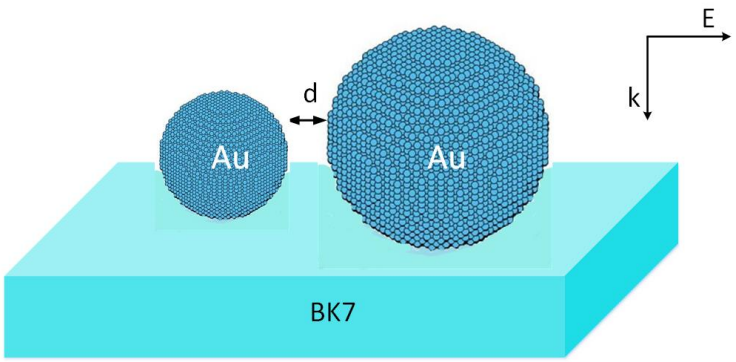


**Figure 39:** Illustration of the Au spherical dimer with different sizes on the BK7 substrate.

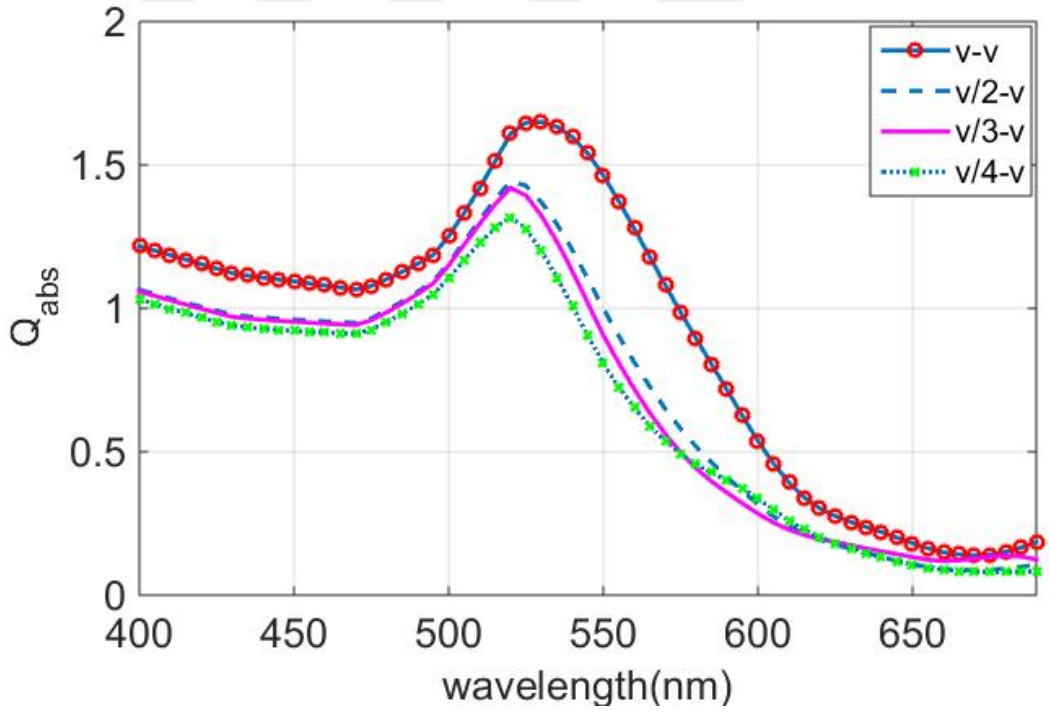


**Figure 40:** Absorption efficiency of the Au nano sphere dimers with different volumes with the fraction of 1/2, 1/3 and 1/4 of the first NP.

In this part, we investigated the absorption efficiency of sphere dimer with different sizes (volume) on BK7 substrate when distances between them is 5 nm, as it has been

shown in Figure 40, it is clear that, the effect of small sphere becomes negligible as the volume of it becomes one-forth of the bigger sphere.

### 5.1.4 Gold oblate nano-sphere with different aspect ratio

In order to investigate the influence of the AuNP geometry on the spectral features of the plasmon resonance, we considered the oblate spheroid AuNP with the major axis $a = 50$ nm (Figure 41) with four different aspect ratios ($b = 1/2a$, $1/3a$, $1/4a$ and $1/5a$). As it is shown in Figure 42 by decreasing the aspect ratio the significant plasmon responses happens; however, the magnitude of absorption efficiency is not changed. It is clear that by increasing the major axis resonance shifted to 580 nm wavelength. The increasing of the available number of electrons per unit volume at the oblate spheroid is the main reason of this resonance.

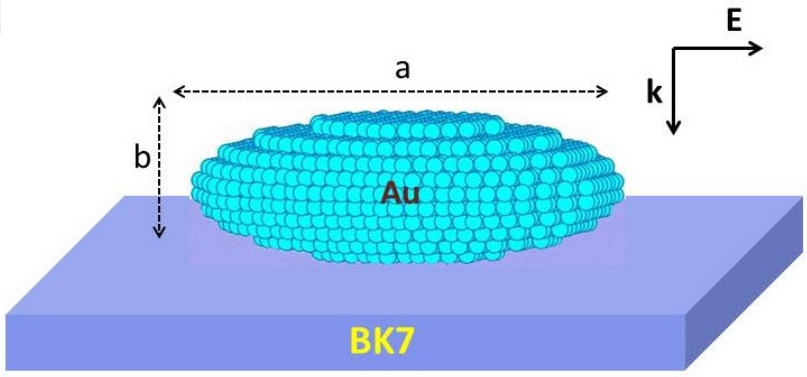


**Figure 41:** Schematic of the model for a single Au oblate nano-sphere on the BK7 substrate.

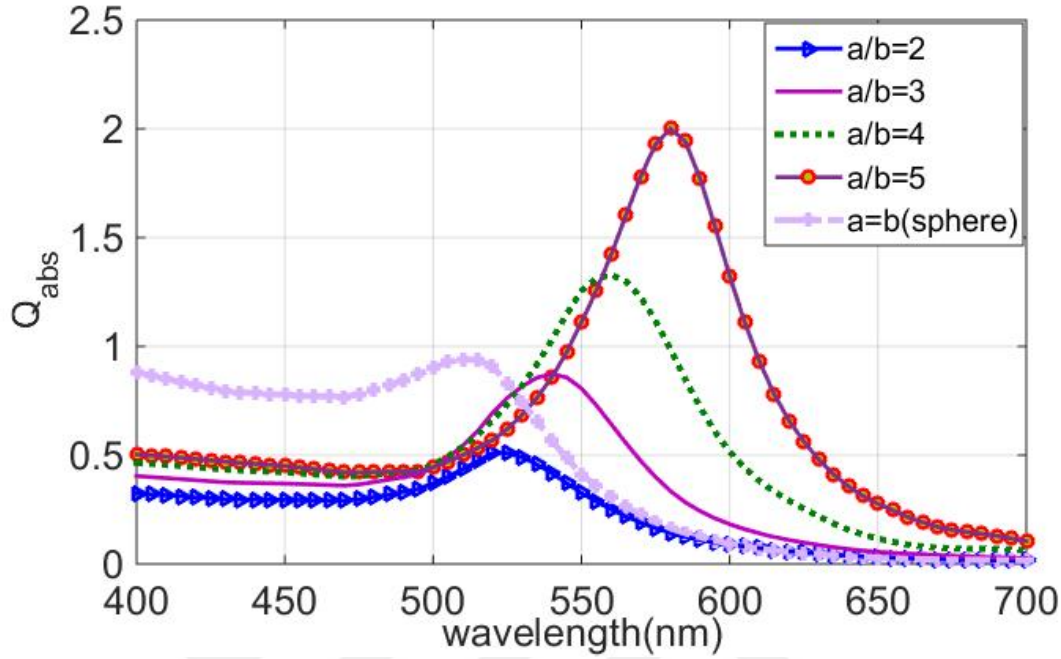


**Figure 42:** Absorption efficiency of a single Au oblate nano-spheres with different aspect ratios( 1/2, 1/3, 1/3 and 1/5)

### 5.1.5 Gold oblate nano-sphere dimers

In the next step, we calculated the absorption efficiency of the oblate spheroid nano-dimer on the BK7 separated by 5 nm ( Figure 43). The major axis of oblate nano-sphere is 50 nm with four different aspect ratios ($b = 1/2a$, $1/3a$, $1/4a$ and $1/5a$). In each calculation, the separation of dimers are kept fixed and just the aspect ratio of the oblates is changed. It is clear from Figure 44 for oblate spheroids as the aspect ratio increased redshifts of the plasmon resonance happens.

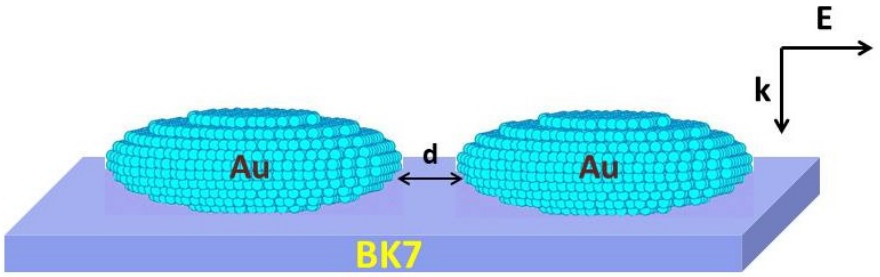


**Figure 43:** Schematic configuration of Au oblate nano-sphere dimer with separation of is 5 nm on the BK7 substrate.

The Figure 44 reveals the characteristic plasmon resonance of Au oblate nano sphere dimers. The high absorption efficiency and plasmon resonance of the oblate nano sphere AuNPs are created due to the increasing the aspect ratio.

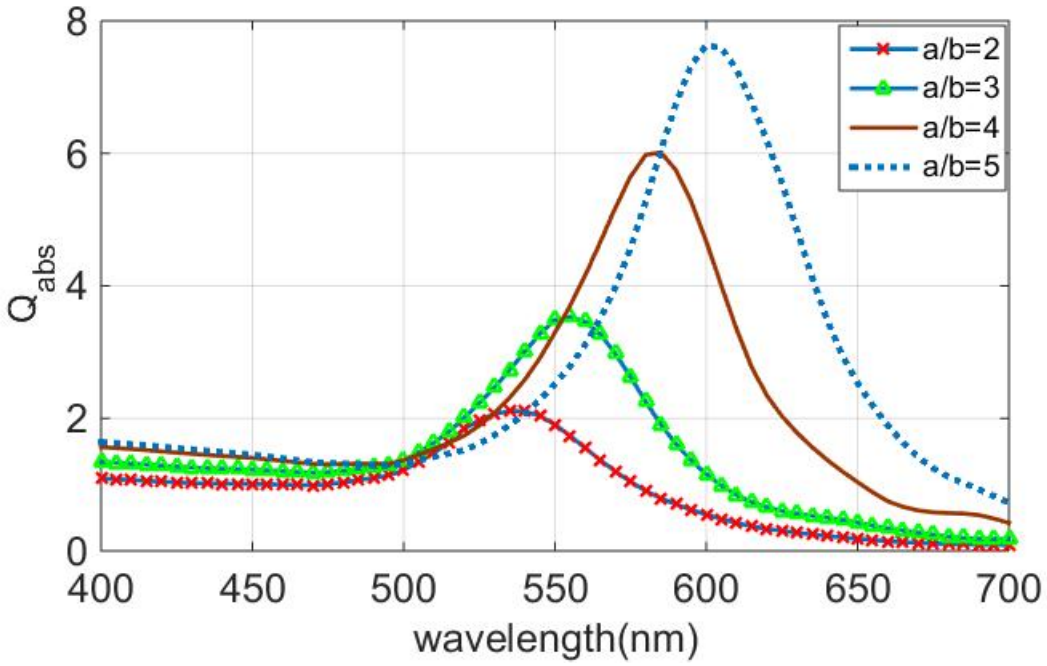


**Figure 44:** Absorption efficiency of Au oblate nano-sphere dimer with 5 nm separation and different aspect ratios ($b = 1/2a$, $1/3a$, $1/4a$ and $1/5a$)

## *5.2 Plasmon Resonance of Cubic Gold Particles*

In this section, we investigated the plasmon resonance of Au nano-cube dimers with different gap separation, different volumes and heights.

### 5.2.1 Dimers of gold nano-cube with different gap separation

Figure 46 is an evidence to the inter particle coupling effects of dimer nano-cube when they are close to each other. Furthermore, as the gap between the particles is increased this effect reduces and thus the absorption spectra approach the spectra of a single sphere as explained in the case 1. It is clear that mutual interaction of the cubes is negligible when the ratio of their distance($d$) to half of cube side ($a$ is side of cube) $c = 2d/a$ is greater than 3. For instance, if the side of the cubes is 50 nm and when the distance becomes 80 nm, the dependent absorption cannot be observed [61][62].

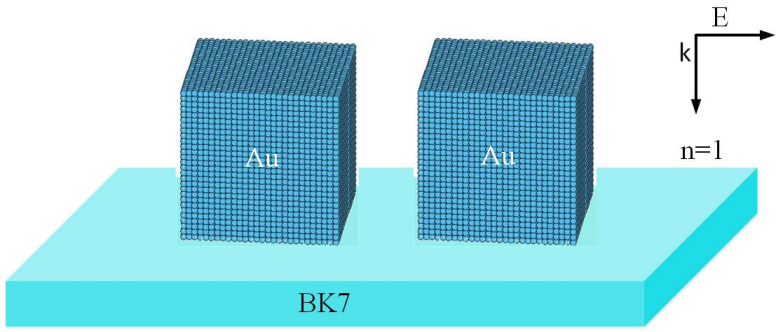


**Figure 45:** Schematic configuration of Au nano-cube dimer with separation of is 5 nm on the BK7 substrate.

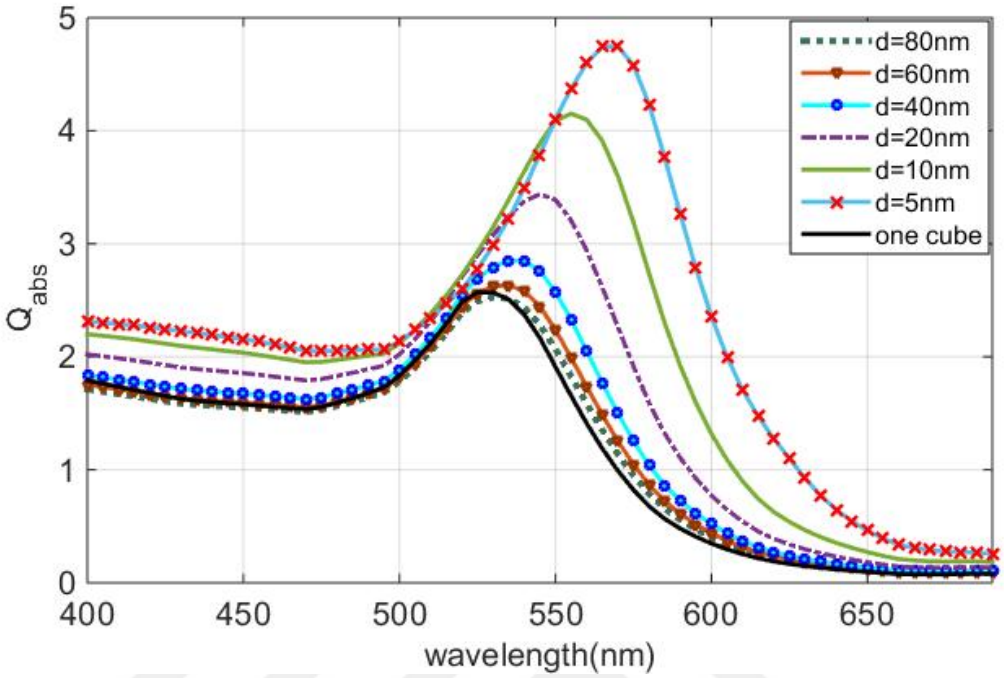


**Figure 46:** Absorption efficiency of Au cubic nano-dimers with different distances compare with single Au nano-cube.

Based on the results of Figure 46 and 47 increasing the distance between nano-cubes will decrease the absorption efficiency and also more interestingly, it causes blue-shift in plasmon resonance frequency and after some point, the response of dimer converge to response of single nano-cube. Electric Field enhancement increases with the decreasing gap destination between AuNPs due to the increase of the charge concentration near the gap.

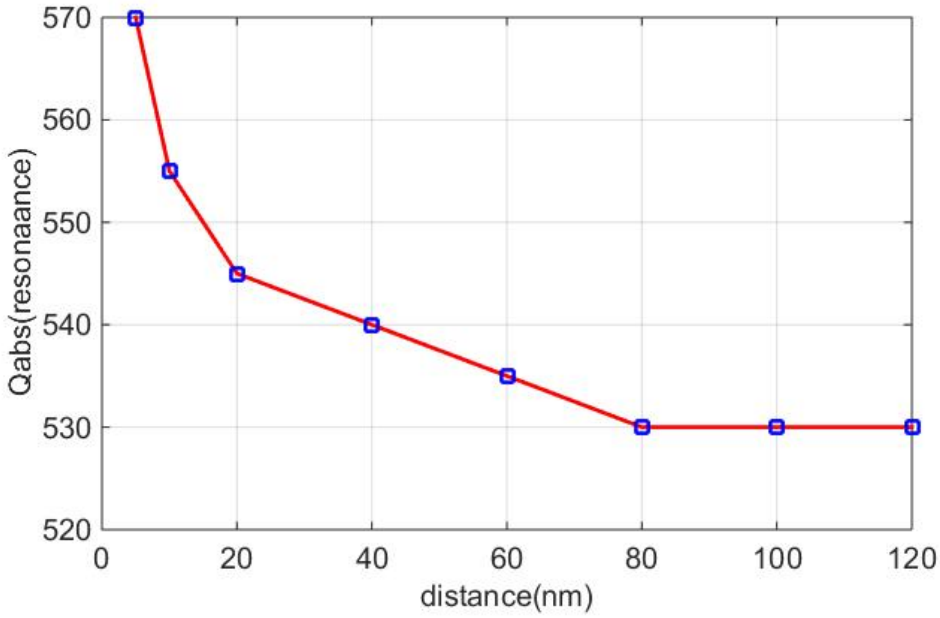


**Figure 47:** Maximum absorption efficiency of the Au nano-cube dimer as a function of their distance.

### 5.2.2 Dimers of gold gano-cube with different height

The absorption efficiency of Au nano-cube dimer in the close proximity (5 nm) when the hight of the second nano-cube is changing is calculated in this part (Figure 48).

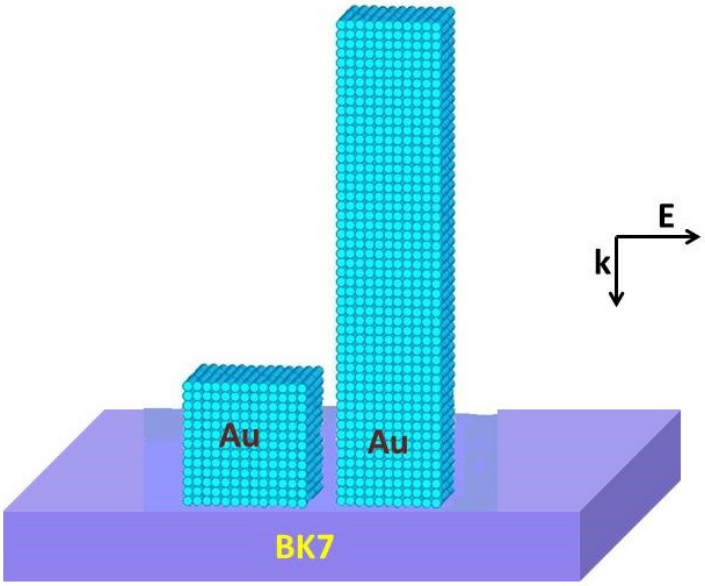


**Figure 48:** Schematic configuration of Au nano-cube dimer with separation of is 5 nm on the BK7 substrate when the hight of the second nano-cube is changing.

The absorption efficiency is increased and it has no influence in plasmon resonance when the hight of the second nano-cube is increased as it is obvious in Figure 49. However, as Figure 49 depicts that when the hight of the second Au nano-cube becomes five times larger that first Au nano- cube, the response of dimer converge to the response of the condition where the hight of the second nano-cube is four times bigger than the first one.

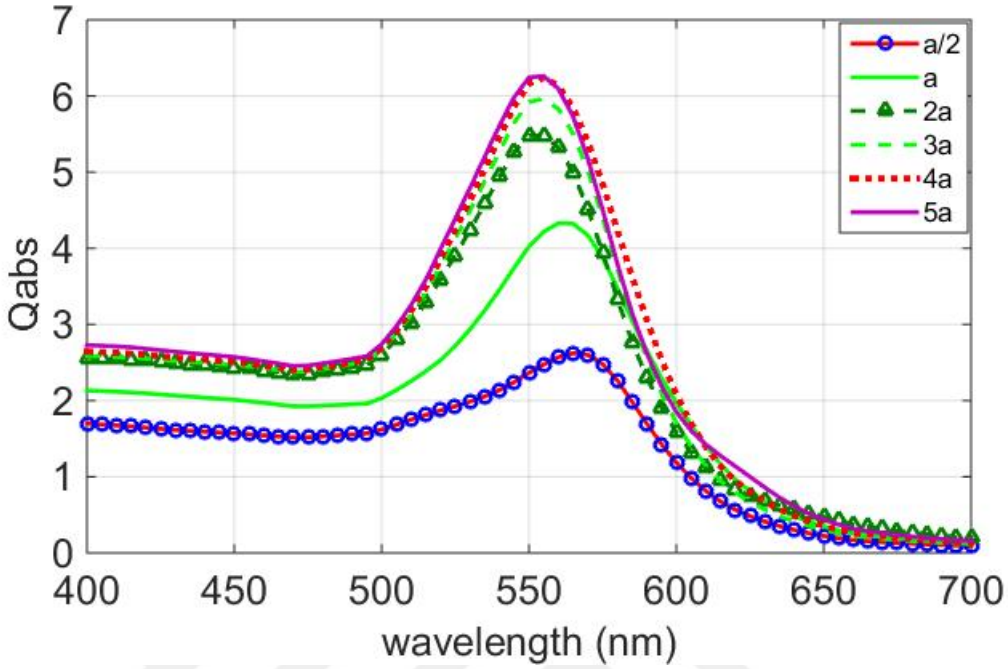


**Figure 49:** Comparison between the absorption efficiency of cubic dimer, when the hight of the second NP is changed.

### 5.2.3 Gold nano-cube with different size

Figure 51 shows what happens to the absorption efficiency of the nano-cube dimmer when the size of the neighboring cubes changes and distance between nano-cubes is 5 nm. The results obtained for the case that electric field incident to the larger cube and then passes to the smaller cube (Figure 50). It is observed that when the volume of smaller cube becomes smaller than 1/5 volume of the bigger one, the influence size changing becomes negligible.

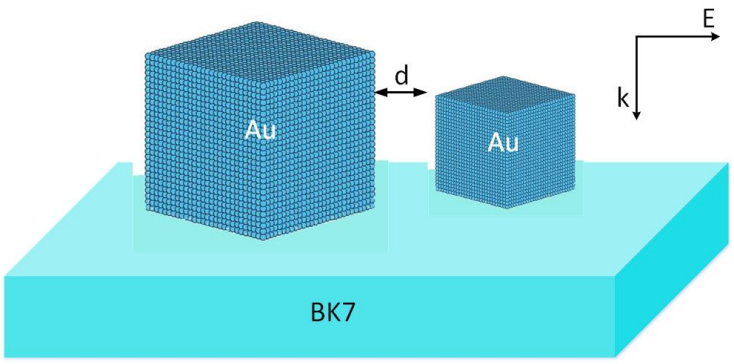


**Figure 50:** Illustration of the Au nano-cube dimmer with different sizes on the BK7 substrate.

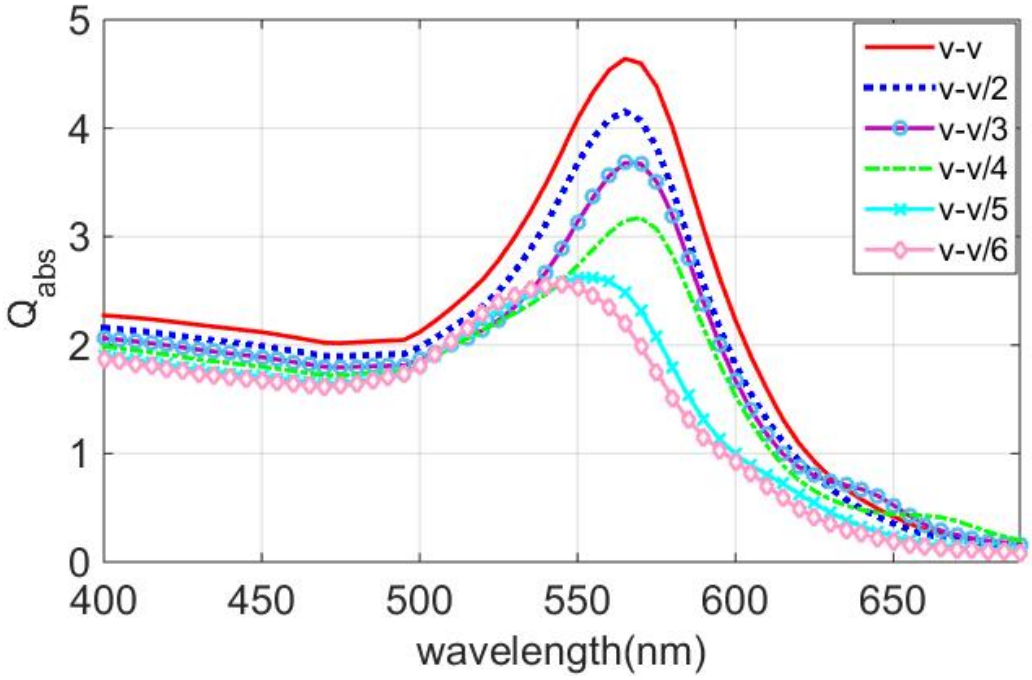


**Figure 51:** Absorption efficiency of the Au nano-cubic dimmer on the BK7 substrate with different volumes.

## *5.3 Dimers of Gold Nano-pyramid and Nano-prism*

To study the effect of the geometry on the value of the plasmon resonance of nano-dimers, we investigated the absorption efficiency of Au nano-pyramid and Au nano-prism on the BK7 substrate. Dimer nanoprisms, also called bowtie structures, are well known from literature [63][64]. The pyramid AuNP base is square and the apex is directly above the center of the base and the prism with sharp and rounded edges ( Figure 52). As it is obvious from Figure 53, the nanoprism dimer have smaller plasmon resonance peak than the pyramid dimer. The plasmon resonance for Au nano-pyramid dimer is shifted to 640 nm meanwhile the resonace for Au bowtie dimer is around 620 nm. Obviously, the shift of pyramid dimer can be explained by increased charge separation of square comparing with triangular which causing an increase in the higher plasmon resonance.

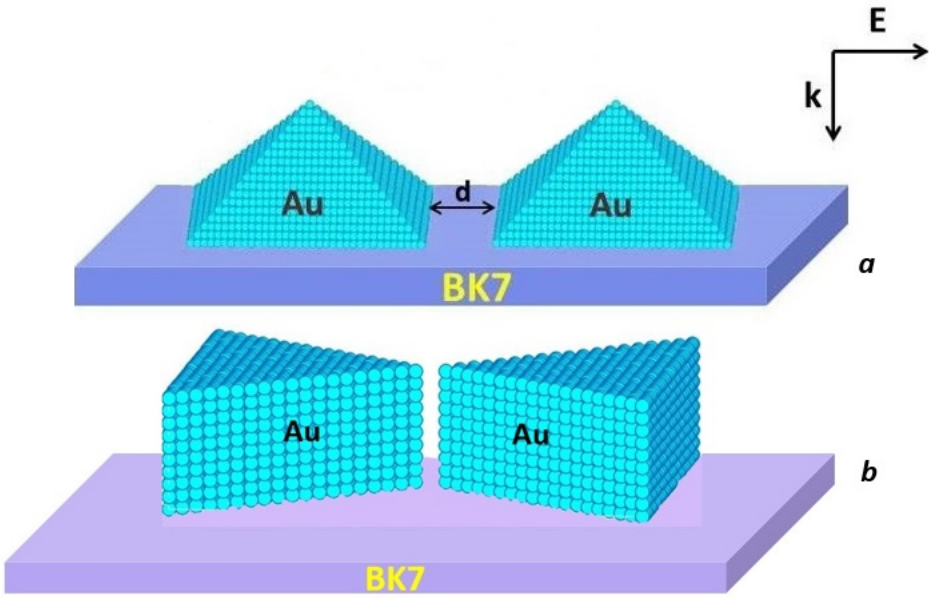


**Figure 52:** Schematic configuration of ($a$) Au nano-pyramid dimer ($b$) Au nano-bowtie with separation of is 5 nm on the BK7 substrate.

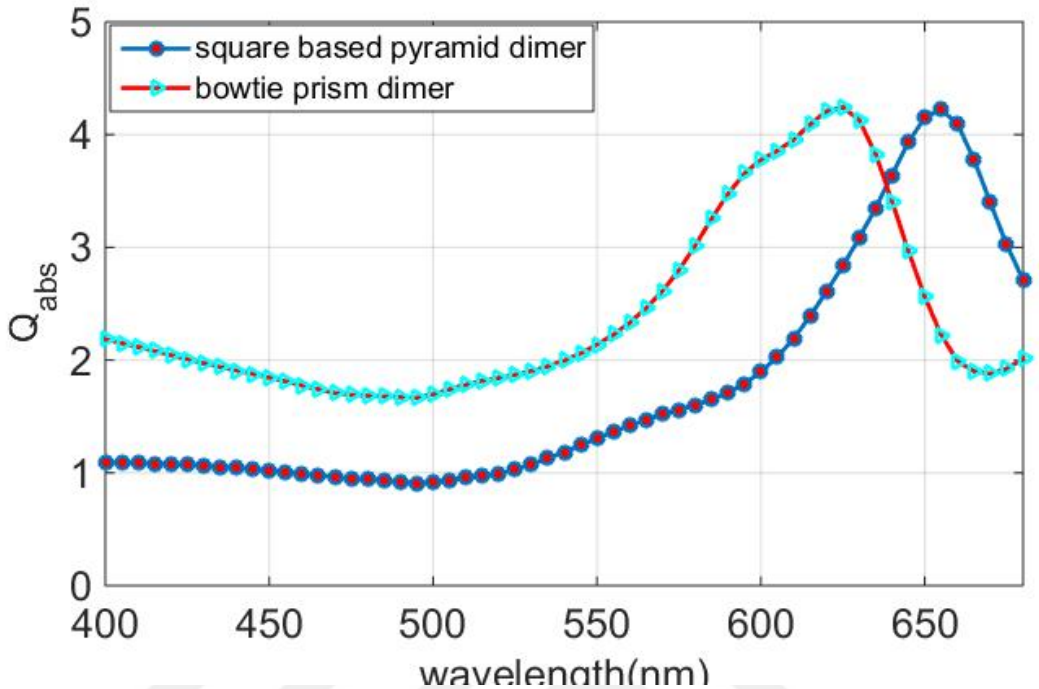


**Figure 53:** Comparison of absorption efficiency between pyramid dimer and bowtie pyramid.

## *5.4 Nano Dimers Formed with Sphere and Cube*

In this thesis, we investigate the response of system for combination of nano-sphere and nano-cube and compare it with results of cube and sphere dimers. Again, for fair comparison, the volume of cube and sphere and also the distance between NPs are kept equal. Figure 55 demonstrates that the absorption efficiency of cube dimer is the highest with the lowest plasmon resonance frequency.

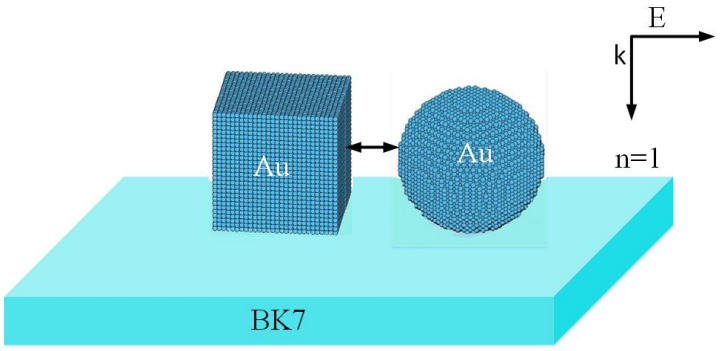


**Figure 54:** Schematic configuration of the Au nano-dimer formed by cube and sphere on the BK7 substrate.

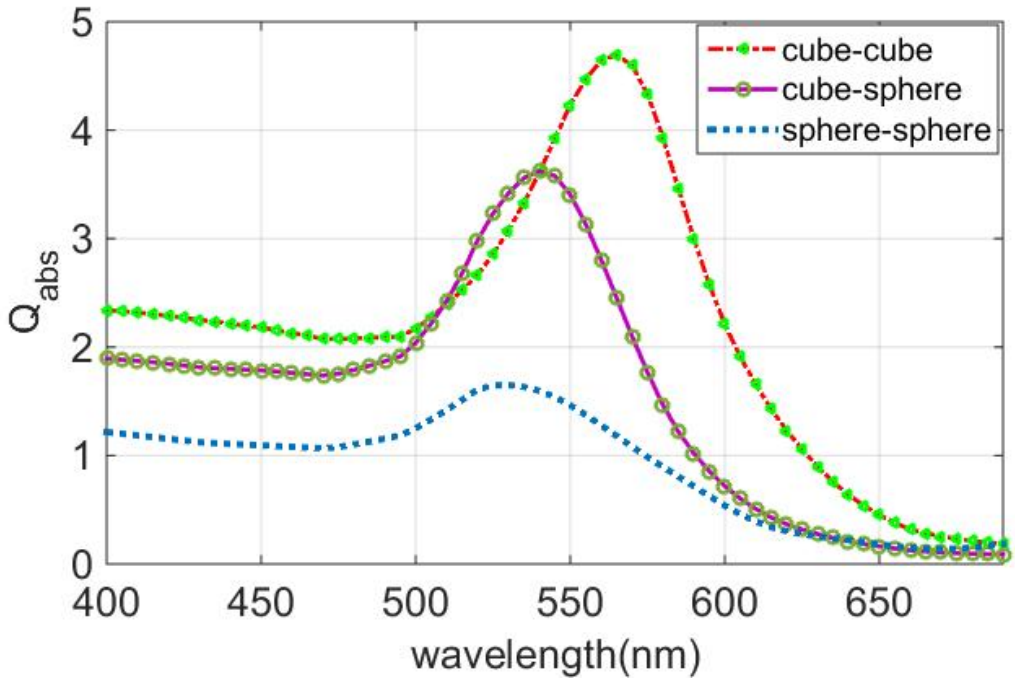


**Figure 55:** Comparison between the absorption efficiency of cubic dimer, spherical dimer and cube-sphere dimer with equal volumes.

## *5.5 Gold Nano-trimers Formed with Sphere and Cube*

In this part of thesis, we investigated the influence of placing of a nano-sphere on plasmon resonance of the adjacent nano-cubes when distances between NPs is 5 nm ( Figure 56). From the Figure 57 it is obvious that the absorption efficiency of Au nano-cube trimer has the maximum absorption efficiency with lowest plasmon resonance frequency. Also when nano-sphere is in the middle of the two nano-cubes, absorption efficiency is the lowest in comparison with other cases.

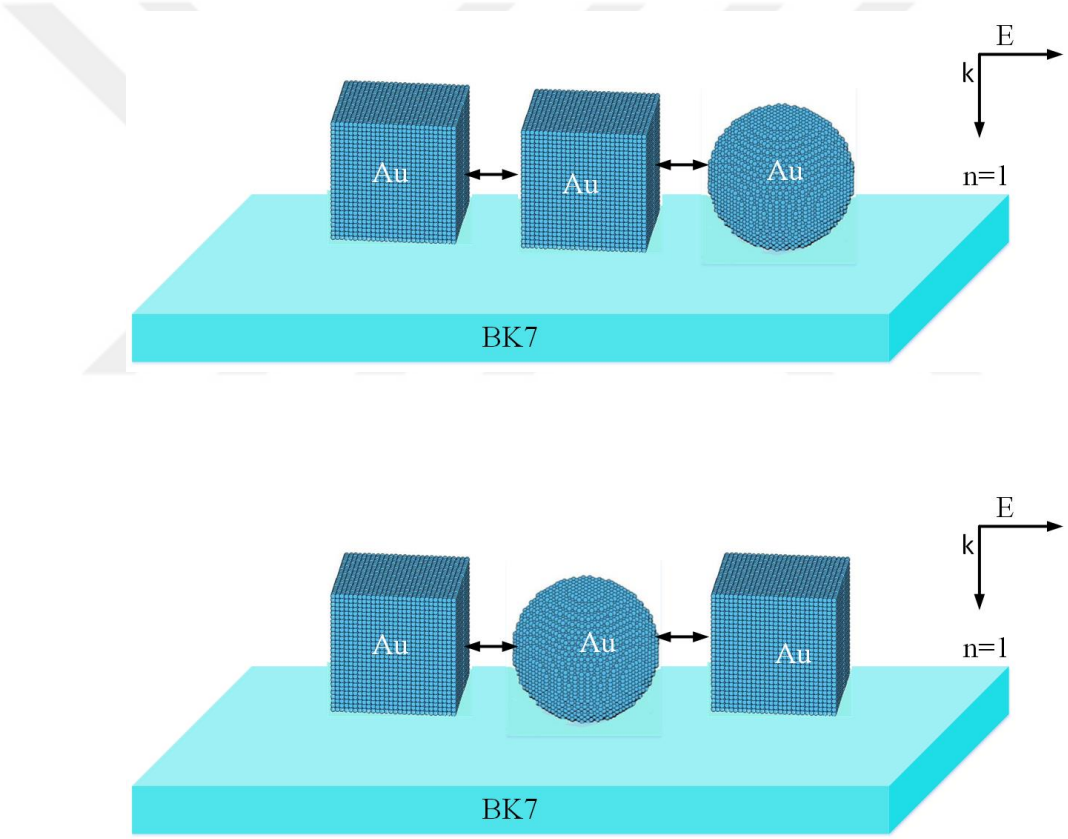


**Figure 56:** Schematic configuration of Au trimers formed by cube and sphere on the BK7 substrate. The trimmer is mixture of two nano-cubes sand one nano-sphere.

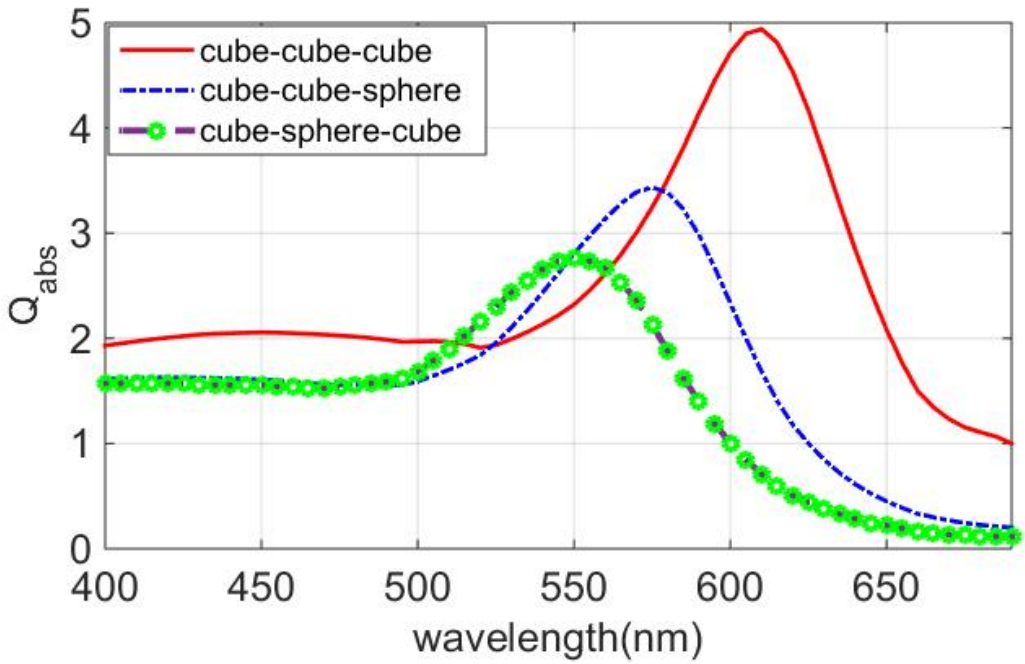


**Figure 57:** Comparison of the absorption efficiency of the Au trimers on the BK7 substrate.

# CHAPTER VI

# DISCUSSION AND CONCULUSIONS

In this work, we calculated optical response of arrays of metallic nano-particles made of gold on the dielectric substrate. The main focus of this study is plasmonics properties and near-field enhancement of such a 3D nanostructurs. The calculations are obtained with DDA-SI toolbox which is an open source MATLAB based software package. These simulations show that DDA-SI can be used for the calculation of scattering and absorption of arrays of gold NPs are affected by the near fields of other particles in their close proximity.

For this purpose, the DDA-SI toolbox is further developed, vectorized $for$ loops of main vDDA-SI toolbox. The new version of toolbox is named zDDA-SI. Furthermore, the main toolbox optimized numerically to provide more precise answers, fast and stable calculation. Because the iterative methods which used in the previous toolboxes(vDDA-SI and sDDA-SI) could not converge to the solution for noble metals. We investigated the construction of interaction matrix in the presence of a substrate. We showed that the total interaction matrix is complex symmetric, well conditioned and it is not a positive definite matrix. Moreover, we find an appropriate iterative method and applied the preconditioning to the iterative solvers in order to solve the linear system of DDA-SI for calculating the moment of each dipole. We have applied three iterative algorithms of GMRES, QMR, and LSQR to solve the linear equations arising in the DDA-SI and we found that LSQR is a suitable iterative method. As the iterative methods converged in relatively high number of iterations for particles with large refractive index, using preconditioning was proposed. We found that LU-decomposition which is built up by decomposition of the total interaction matrix as

a preconditioner could speed up the iterative calculation by decreasing the iteration numbers in the LSQR iterative solver. We proved that LU-LSQR method converges to the solution within two steps of iteration and has the residual errors on the order of $10^{-7}$-$10^{-10}$ for AuNPs.

Furthermore, we showed that the numerical errors within DDA-SI can be reduced by choosing a small dipole size (lattice spacing) for noble metals and appropriate iterative methods (LSQR) with high tolerance values. We demonstrated that the performance of iterative solvers largely depends on the refractive index and geometry of particles. We also prove that our method is stable for light scattering calculation and it is converging for the noble materials whose imaginary part refractive index is high in the larger wavelengths in the spectrum.

Moreover, we have presented that there is an artificial plasmon resonance around (wavelength 620 nm) for spherical particles due to the shape error when number of dipoles is lower than 280 (dipole size $> 0.02$ ) due to lack of DDA-SI criteria: $d \leq 1/|m|k$. We concluded that, the minimum number of dipoles required for proper discretization of spherical geometries. However, for complex geometries such as pyramid in order to simulate them precisely, the large number of dipole is desired. For summary in the case of the sufficient dipole numbers for different AuNPs geometries, cube comprises the most simple geometry, therefore, accurate calculation could achieve by lower number of dipoles and also the errors for cube is the minimum comparing with other maintained geometries.

In addition, We investigated that the plasmon resonance and the absorption efficiency of the AuNPs arrays on the BK7 substrate depend on the geometry of the particles and gap distance between them. We found out that as the distance of NPs decreases, the plasmon resonance frequency is pushed into the infrared region due to the inter-particle coupling so the red-shift becomes dominant. Small changes in the geometry of noble metals and distribution of them can have effects on the absorption

profiles and near field patterns. It is worth to mention that AuNPs with different shapes in array configurations show the greater promise in the absorption efficiency. Also, cube are highly tunable than sphere, and can be made to absorb in the visible light spectrum preferentially. As well as, the oblate spheroid AuNPs are more tunable than nano-spheres, as the ratio of the axes becomes larger the plasmon resonance band shifted to infrared. Pyramid shaped NPs shows highly tunable near-field plasmonic behaviors than other geometries.

In summary, we have calculated the resonance modes for different plasmonic nanostructures of Au dimer(including sphere, oblate nano sphere, cube and pyramid). We conclude that cubes and pyramids due to the inter coupling in the dimers shows the tunable plasmon resonance behavior than other geometries. Overall, we investigated the absorption efficiency of trimers which formed with Au nano-sphere and nano-cubes. We conclude that interaction of Au nano sphere with nano-cubes in trimer cause to reduce the plasmon mode to ultraviolet bands and blue shifted become dominant.

# Bibliography


[1] P. B. Johnson and R.-W. Christy, "Optical constants of the noble metals," *Physical review B*, vol. 6, no. 12, p. 4370, 1972.

[2] V. L. Loke, M. P. Mengüç, and T. A. Nieminen, "Discrete-dipole approximation with surface interaction: Computational toolbox for matlab," *Journal of Quantitative Spectroscopy and Radiative Transfer*, vol. 112, no. 11, pp. 1711–1725, 2011.

[3] S. T. Moghaddam, H. Ertürk, and M. P. Mengüç, "Enhancing local absorption within a gold nano-sphere on a dielectric surface under an afm probe," *Journal of Quantitative Spectroscopy and Radiative Transfer*, vol. 178, pp. 124–133, 2016.

[4] V. L. Y. Loke and M. P. Mengüç, "Surface waves and atomic force microscope probe-particle near-field coupling: discrete dipole approximation with surface interaction.," *Journal of the Optical Society of America. A, Optics, image science, and vision*, vol. 27, no. 10, pp. 2293–2303, 2010.

[5] Q. Jiang, H. Tong, D. Hsu, K. Okuyama, and F. Shi, "Thermal stability of crystalline thin films," *Thin Solid Films*, vol. 312, no. 1-2, pp. 357–361, 1998.

[6] S. K. Ghosh and T. Pal, "Interparticle coupling effect on the surface plasmon resonance of gold nanoparticles: From theory to applications," *Chemical Reviews*, vol. 107, no. 11, pp. 4797–4862, 2007.

[7] S. A. Maier, *Plasmonics: fundamentals and applications*. Springer Science & Business Media, 2007.

[8] B. Luk'yanchuk, N. I. Zheludev, S. a. Maier, N. J. Halas, P. Nordlander, H. Giessen, and C. T. Chong, "The Fano resonance in plasmonic nanostructures and metamaterials.," *Nature materials*, vol. 9, no. 9, pp. 707–15, 2010.

[9] A. Verma and F. Stellacci, "Effect of surface properties on nanoparticle-cell interactions," *Small*, vol. 6, no. 1, pp. 12–21, 2010.

[10] X.-M. Zhang, J.-J. Xiao, and Q. Zhang, "Optical binding forces between plasmonic nanocubes: A numerical study based on discrete-dipole approximation," *Chinese Physics B*, vol. 23, no. 1, p. 017302, 2014.

[11] M. A. El-Sayed, "Some interesting properties of metals confined in time and nanometer space of different shapes," *Accounts of Chemical Research*, vol. 34, no. 4, pp. 257–264, 2001.

[12] B. T. Wong and M. P. Mengüç, *Thermal Transport for Applications in Micro/Nanomachining*. Springer Science & Business Media, 2008.

[13] E. A. Hawes, J. T. Hastings, C. Crofcheck, and M. P. Mengüç, "Spectrally selective heating of nanosized particles by surface plasmon resonance," *Journal of Quantitative Spectroscopy and Radiative Transfer*, vol. 104, no. 2, pp. 199–207, 2007.

[14] A. O. Govorov, W. Zhang, T. Skeini, H. Richardson, J. Lee, and N. A. Kotov, "Gold nanoparticle ensembles as heaters and actuators: Melting and collective plasmon resonances," *Nanoscale Research Letters*, vol. 1, no. 1, pp. 84–90, 2006.

[15] M. Francoeur and M. P Mengüç, "Role of fluctuational electrodynamics in near-field radiative heat transfer," *Journal of Quantitative Spectroscopy and Radiative Transfer*, vol. 109, no. 2, pp. 280–293, 2008.

[16] P. K. Jain, Y. Xiao, R. Walsworth, and A. E. Cohen, "Surface Plasmon Resonance Enhanced Rotation Enhancement in Gold-Coated Iron Oxide Nanocrystals," *Nano Letters*, vol. 9, no. 4, p. 1644, 2009.

[17] T. Som and B. Karmakar, "Surface plasmon resonance in nano-gold antimony glass-ceramic dichroic nanocomposites: One-step synthesis and enhanced fluorescence application," *Applied Surface Science*, vol. 255, no. 23, pp. 9447–9452, 2009.

[18] E. C. Le Ru, P. G. Etchegoin, and M. Meyer, "Enhancement factor distribution around a single surface-enhanced Raman scattering hot spot and its relation to single molecule detection," *Journal of Chemical Physics*, vol. 125, no. 20, pp. 1–14, 2006.

[19] S. J. Barrow, X. Wei, J. S. Baldauf, A. M. Funston, and P. Mulvaney, "The surface plasmon modes of self-assembled gold nanocrystals.," *Nature communications*, vol. 3, p. 1275, 2012.

[20] C. Ungureanu, R. G. Rayavarapu, S. Manohar, and T. G. Van Leeuwen, "Discrete dipole approximation simulations of gold nanorod optical properties: Choice of input parameters and comparison with experiment," *Journal of Applied Physics*, vol. 105, no. 10, 2009.

[21] P. Yang and K. N. Liou, "Finite-difference time domain method for light scattering by small ice crystals in three-dimensional space," *J. Opt. Soc. Am. A*, vol. 13, pp. 2072–2085, Oct 1996.

[22] C. S. Levin, C. Hofmann, T. a. Ali, a. T. Kelly, E. Morosan, P. Nordlander, K. H. Whitmire, and N. J. Halas, "Magnetic Plasmonic Core Shell Nanoparticles," *ACS nano*, vol. 3, no. 6, pp. 1379–1388, 2009.

[23] B. T. Draine and P. J. Flatau, "Discrete-dipole approximation for scattering calculations," *JOSA A*, vol. 11, no. 4, pp. 1491–1499, 1994.

[24] M. A. Yurkin and A. G. Hoekstra, "User manual for the discrete dipole approximation code adda 1.3 b4," 2014.

[25] M. I. Mishchenko, J. W. Hovenier, and L. D. Travis, *Light scattering by nonspherical particles: theory, measurements, and applications*. Academic press, 1999.

[26] A. Taflove and S. C. Hagness, *Computational electrodynamics: the finite-difference time-domain method*. Artech house, 2005.

[27] T. Wriedt *et al.*, "A review of elastic light scattering theories," *Particle & particle systems characterization*, vol. 15, no. 2, pp. 67–74, 1998.

[28] K.-N. Liou and P. Yang, *Light scattering by ice crystals: fundamentals and applications*. Cambridge University Press, 2016.

[29] P. C. Waterman, "Symmetry, unitarity, and geometry in electromagnetic scattering," *Physical review D*, vol. 3, no. 4, p. 825, 1971.

[30] V. L. Loke, G. Huda, E. Donev, V. Schmidt, J. Hastings, M. P. Mengüç, and T. Wriedt, "Comparison between discrete dipole approximation and other modelling methods for the plasmonic response of gold nanospheres," *Applied Physics B*, vol. 115, no. 2, pp. 237–246, 2014.

[31] R. Schmehl, "The coupled-dipole method for light scattering from particles on plane surfaces," *Arizona State University, Dept. of Mechanical and Aerospace Engineering*, 1994.

[32] H. DeVoe, "Optical properties of molecular aggregates. i. classical model of electronic absorption and refraction," *The Journal of chemical physics*, vol. 41, no. 2, pp. 393–400, 1964.

[33] E. M. Purcell and C. R. Pennypacker, "Scattering and absorption of light by nonspherical dielectric grains," *The Astrophysical Journal*, vol. 186, pp. 705–714, 1973.

[34] M. J. Collinge and B. Draine, "Discrete-dipole approximation with polarizabilities that account for both finite wavelength and target geometry," *JOSA A*, vol. 21, no. 10, pp. 2023–2028, 2004.

[35] J. Mc Donald, A. Golden, and S. G. Jennings, "Opendda: a novel high-performance computational framework for the discrete dipole approximation," *International Journal of High Performance Computing Applications*, vol. 23, no. 1, pp. 42–61, 2009.

[36] M. A. Yurkin and A. G. Hoekstra, "The discrete dipole approximation: an overview and recent developments," *Journal of Quantitative Spectroscopy and Radiative Transfer*, vol. 106, no. 1, pp. 558–589, 2007.

[37] M. A. Taubenblatt and T. K. Tran, "Calculation of light scattering from particles and structures on a surface by the coupled-dipole method," *JOSA A*, vol. 10, no. 5, pp. 912–919, 1993.

[38] R. Schmehl, B. M. Nebeker, and E. D. Hirleman, "Discrete-dipole approximation for scattering by features on surfaces by means of a two-dimensional fast fourier transform technique," *JOSA A*, vol. 14, no. 11, pp. 3026–3036, 1997.

[39] M. A. Yurkin and M. Huntemann, "Rigorous and fast discrete dipole approximation for particles near a plane interface," *The Journal of Physical Chemistry C*, vol. 119, no. 52, pp. 29088–29094, 2015.

[40] S. Manickavasagam and M. Mengüç, "Scattering matrix elements of fractal-like soot agglomerates," *Applied Optics*, vol. 36, no. 6, pp. 1337–1351, 1997.

[41] M. R. Short, J.-M. Geffrin, R. Vaillon, H. Tortel, B. Lacroix, and M. Francoeur, "Evanescent wave scattering by particles on a surface: Validation of the discrete dipole approximation with surface interaction against microwave analog experiments," *Journal of Quantitative Spectroscopy and Radiative Transfer*, vol. 146, pp. 452–458, 2014.

[42] J. McDonald, A. Golden, and S. G. Jennings, "Opendda: a Novel High-Performance Computational Framework for the Discrete Dipole Approximation," *International Journal of High Performance Computing Applications*, vol. 23, no. 1, pp. 42–61, 2009.

[43] R. Schmehl, B. M. Nebeker, and E. D. Hirleman, "Discrete-dipole approximation for scattering by features on surfaces by means of a two-dimensional fast Fourier transform technique," *Journal of the Optical Society of America A*, vol. 14, no. 11, p. 3026, 1997.

[44] M. A. Ordal, R. J. Bell, R. W. Alexander, L. L. Long, and M. R. Querry, "Optical properties of fourteen metals in the infrared and far infrared: Al, co, cu, au, fe, pb, mo, ni, pd, pt, ag, ti, v, and w.," *Applied optics*, vol. 24, no. 24, pp. 4493–4499, 1985.

[45] J. R. Howell, M. P. Menguc, and R. Siegel, *Thermal radiation heat transfer*. CRC press, 2016.

[46] A. Vial and T. Laroche, "Comparison of gold and silver dispersion laws suitable for fdtd simulations," *Applied Physics B*, vol. 93, no. 1, pp. 139–143, 2008.

[47] P. Drude, *The theory of optics*. Courier Corporation, 1925.

[48] B. T. Draine, "The discrete-dipole approximation and its application to interstellar graphite grains," *The Astrophysical Journal*, vol. 333, pp. 848–872, 1988.

[49] B. T. Draine and J. Goodman, "Beyond clausius-mossotti-wave propagation on a polarizable point lattice and the discrete dipole approximation," *The Astrophysical Journal*, vol. 405, pp. 685–697, 1993.

[50] S. T. Moghaddam, D. Avşar, H. Ertürk, and M. P. Mengüç, "Effect of the probe location on the absorption by an array of gold nano-particles on a dielectric surface," *Journal of Quantitative Spectroscopy and Radiative Transfer*, 2017.

[51] A. Sommerfeld, "Über die ausbreitung der wellen in der drahtlosen telegraphie," *Annalen der Physik*, vol. 333, no. 4, pp. 665–736, 1909.

[52] W. H. Press, S. A. Teukolsky, W. T. Vetterling, and B. P. Flannery, *Numerical recipes in C*, vol. 2. Cambridge university press Cambridge, 1996.

[53] Z. Bai, J. Demmel, J. Dongarra, A. Ruhe, and H. van der Vorst, *Templates for the solution of algebraic eigenvalue problems: a practical guide*, vol. 11. Siam, 2000.

[54] P. Flatau, "Fast solvers for one dimensional light scattering in the discrete dipole approximation," *Optics express*, vol. 12, no. 14, pp. 3149–3155, 2004.

[55] M. A. Yurkin, M. Min, and A. G. Hoekstra, "Application of the discrete dipole approximation to very large refractive indices: Filtered coupled dipoles revived," *Physical Review E*, vol. 82, no. 3, p. 036703, 2010.

[56] K. Lumme and J. Rahola, "Light scattering by porous dust particles in the discrete-dipole approximation," *The Astrophysical Journal*, vol. 425, pp. 653–667, 1994.

[57] J. Rahola, "Solution of dense systems of linear equations in the discrete-dipole approximation," *SIAM Journal on Scientific Computing*, vol. 17, no. 1, pp. 78–89, 1996.

[58] R. B. Berry, T. F. Chan, J. Demmel, J. M. Donato, J. Dongarra, V. Eijkhout, R. Pozo, C. Romine, and H. Van der Vorst10, "Templates for the solution of linear systems: Building blocks for iterative methods1," *Society for Industrial Mathematics*, 1987.

[59] G. M. Huda, E. U. Donev, M. P. Mengüç, and J. T. Hastings, "Effects of a silicon probe on gold nanoparticles on glass under evanescent illumination.," *Optics express*, vol. 19, no. 13, pp. 12679–12687, 2011.

[60] M. Morgan and K. Mei, "Finite-element computation of scattering by inhomogeneous penetrable bodies of revolution," *IEEE Transactions on Antennas and Propagation*, vol. 27, no. 2, pp. 202–214, 1979.

[61] Z. Ivezić and M. P. Mengüç, "An investigation of dependent/independent scattering regimes using a discrete dipole approximation," *International Journal of Heat and Mass Transfer*, vol. 39, no. 4, pp. 811–822, 1996.

[62] C. Klusek, S. Manickavasagam, and M. P. Mengüç, "Compendium of scattering matrix element profiles for soot agglomerates," *Journal of Quantitative Spectroscopy and Radiative Transfer*, vol. 79, pp. 839–859, 2003.

[63] J. Ye and P. Van Dorpe, "Plasmonic behaviors of gold dimers perturbed by a single nanoparticle in the gap," *Nanoscale*, vol. 4, no. 22, pp. 7205–7211, 2012.

[64] A. Didari and M. P. Menguc, "A design tool for near-field radiative transfer: The developmental steps of the nf-rt-fdtd code," in *ICHMT DIGITAL LIBRARY ONLINE*, Begel House Inc., 2016.

# VITA

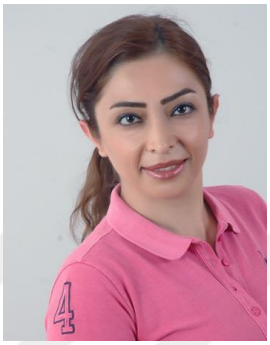

**Zahra Rostampour Fathi** received his B.Sc. degree in Applied Physics in 2004 from University of Tabriz, Tabriz, Iran. In 2013, she joined to the Mechanical Engineering Department and to Center for Energy, Environment and Economy ($CEEE$) at Özyegin University and worked. Her research interests are mostly on the light scattering simulations from particles and plasmonic.